


ARTICLE

Gilgamesh (Gish)/CK1 γ regulates tissue homeostasis and aging in adult *Drosophila* midgut

Shuangxi Li^{1*}, Aiguo Tian^{1,2*}, Shuang Li^{1,2*}, Yuhong Han^{1,2}, Bing Wang^{1,2}, and Jin Jiang^{1,2,3} 

Adult tissues and organs rely on resident stem cells to generate new cells that replenish damaged cells. To maintain homeostasis, stem cell activity needs to be tightly controlled throughout the adult life. Here, we show that the membrane-associated kinase Gilgamesh (Gish)/CK1 γ maintains *Drosophila* adult midgut homeostasis by restricting JNK pathway activity and that Gish is essential for intestinal stem cell (ISC) maintenance under stress conditions. Inactivation of Gish resulted in aberrant JNK pathway activation and excessive production of multiple cytokines and growth factors that drive ISC overproliferation. Mechanistically, Gish restricts JNK activation by phosphorylating and destabilizing a small GTPase, Rho1. Interestingly, we find that Gish expression is down-regulated in aging guts and that increasing Gish activity in aging guts can restore tissue homeostasis. Hence, our study identifies Gish/CK1 γ as a novel regulator of Rho1 and gatekeeper of tissue homeostasis whose activity is compromised in aging guts.

Introduction

During adult life of multicellular organisms, stem cells reside in many organs and constantly produce new cells to replenish damaged cells in order to maintain tissue homeostasis and organ function; however, the regulatory mechanisms that control stem cell maintenance, proliferation, and differentiation are not fully understood. *Drosophila melanogaster* adult midgut has emerged as an attractive system to study stem cell biology in adult tissue homeostasis and regeneration because of its relatively simple and well-characterized stem cell lineage and easy accessibility to genetic manipulation (Biteau et al., 2011; Jiang and Edgar, 2012; Jiang et al., 2016).

Drosophila posterior midgut contains self-renewing intestinal stem cells (ISCs) located at the basal side of the midgut epithelium adjacent to the basement membrane (Micchelli and Perrimon, 2006; Ohlstein and Spradling, 2006). An ISC normally undergoes asymmetric cell division to produce a renewed ISC and either an enteroblast (EB) that differentiates into an absorptive enterocyte (EC) or a pre-enteroendocrine cell that differentiates into a secretory enteroendocrine cell (Fig. 1 A; Ohlstein and Spradling, 2007; Goulas et al., 2012; Biteau and Jasper, 2014; Tian and Jiang, 2014; Beehler-Evans and Micchelli, 2015; Zeng and Hou, 2015; Chen et al., 2018). The asymmetric fate determination of ISC daughters in the EC lineage is controlled by the Par/atypical PKC/integrin-directed apical-basal

cell division and epithelium-derived bone morphogenetic protein that promotes asymmetric Notch pathway activity in the ISC daughter cells (Goulas et al., 2012; Tian and Jiang, 2014; Tian and Jiang, 2017).

Compared with mammalian intestines, ISCs in *Drosophila* adult midguts are relatively quiescent under the homeostatic condition; however, tissue stress and injury can dramatically increase the rate of ISC proliferation and differentiation, allowing a rapid replenishment of damaged cells (Biteau et al., 2011; Jiang and Edgar, 2012; Jiang et al., 2016). A number of signaling pathways, including insulin, JNK, Janus kinase (JAK)-signal transducer and transcription factor (STAT), EGF receptor (EGFR), Hippo, Wingless (Wg)/Wnt, bone morphogenetic protein, and Hedgehog, have been implicated in the regulation of ISC proliferation during midgut homeostasis and regeneration (Amcheslavsky et al., 2009; Buchon et al., 2009; Jiang et al., 2009, 2011; Lee et al., 2009; Karpowicz et al., 2010; Ren et al., 2010; Shaw et al., 2010; Biteau and Jasper, 2011; Xu et al., 2011; Cordero et al., 2012; Guo et al., 2013; Li et al., 2013; Tian et al., 2015, 2017). How these pathways are regulated under normal homeostasis or in response to tissue damage and how they are integrated to control stem cell proliferation and differentiation are still not well understood.

¹Department of Developmental Biology, University of Texas Southwestern Medical Center, Dallas, TX; ²Department of Molecular Biology, University of Texas Southwestern Medical Center, Dallas, TX; ³Department of Pharmacology, University of Texas Southwestern Medical Center, Dallas, TX.

*Shuangxi Li, Aiguo Tian, and Shuang Li contributed equally to this paper; Correspondence to Jin Jiang: jin.jiang@utsouthwestern.edu; Shuangxi Li's present address is Department of Pathology, Stanford University School of Medicine, Stanford, CA.

© 2020 Li et al. This article is distributed under the terms of an Attribution-Noncommercial-Share Alike-No Mirror Sites license for the first six months after the publication date (see <http://www.rupress.org/terms/>). After six months it is available under a Creative Commons License (Attribution-Noncommercial-Share Alike 4.0 International license, as described at <https://creativecommons.org/licenses/by-nc-sa/4.0/>).

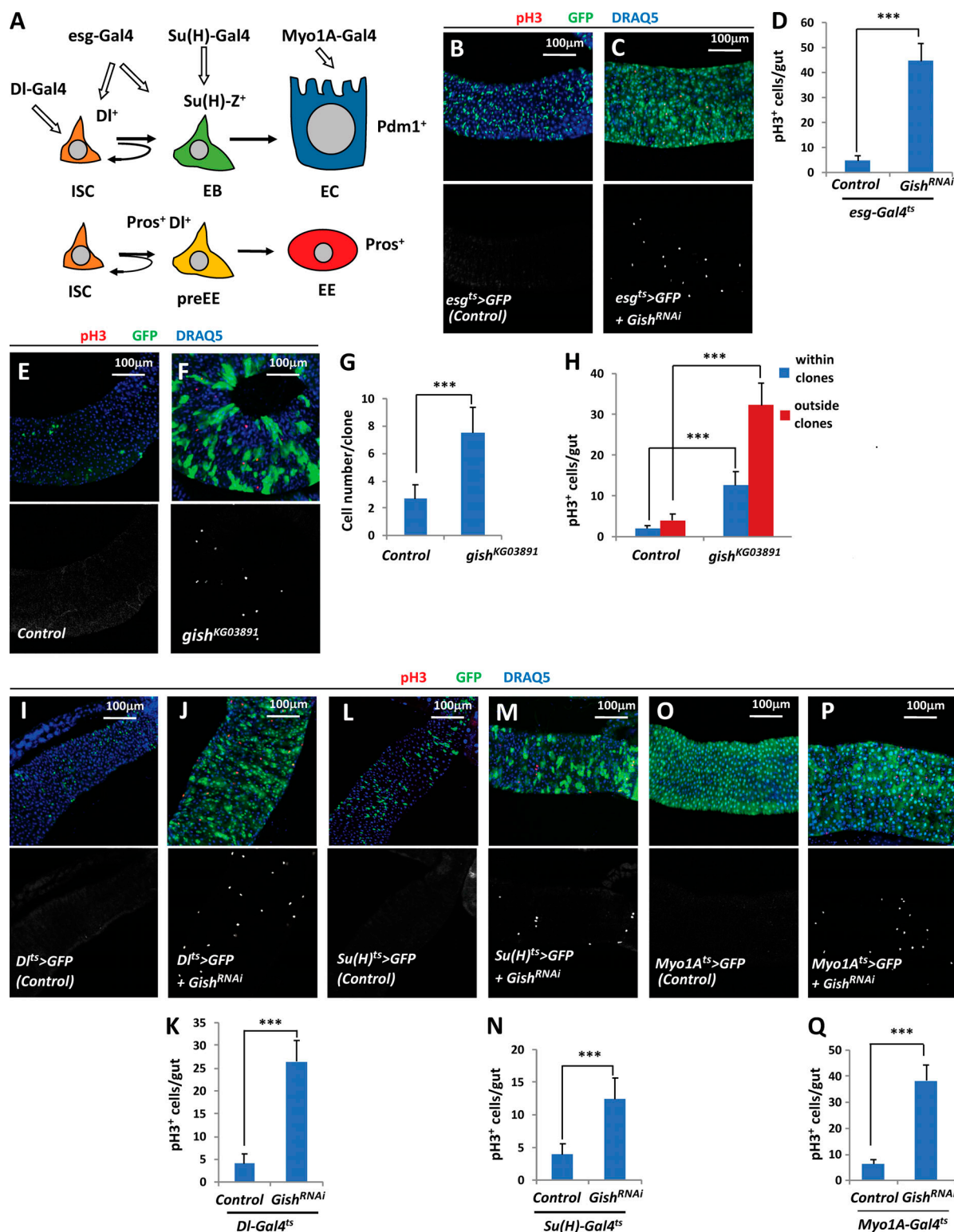


Figure 1. Gish restricts ISC proliferation in *Drosophila* midgut. **(A)** ISC lineage in *Drosophila* adult midgut. **(B–D)** 2–3-d-old adult females of *esg^{ts}* control or *gish^{RNAi}* were shifted to 29°C for 7 d, followed by immunostaining for GFP, pH3, and DRAQ5. Of note, pH3 staining is also shown in black-and-white single channel in this and the following figures. Quantification of pH3⁺ cells is shown in D. Three independent experiments were performed. $n = 30$ guts for each genotype. Data are mean \pm SD. *** $P < 0.001$ (Student's t test). **(E and F)** Midguts containing MACRM clones for *FRT82B* control or *FRT82B gish^{KG03891}* were immunostained for pH3 (red), GFP (green), and DRAQ5 (blue) at 7 d after clonal induction. **(G and H)** Quantification of clone size (G) and number of pH3⁺ cells inside and outside the control or *gish* mutant clones (H). $n = 18$ guts for each genotype. Data are mean \pm SD. *** $P < 0.001$ (Student's t test). **(I–Q)** 2–3-d-old adult females expressing the indicated Gal4 driver and UAS-GFP without (I, L, and O) or with (J, M, and P) *Gish^{RNAi}* were shifted to 29°C for 7 d, followed by immunostaining for GFP, pH3, and DRAQ5. Quantification of pH3⁺ cells is shown in K, N, and Q. $n = 20$ guts for each genotype. Data are mean \pm SD. *** $P < 0.001$ (Student's t test).

To identify new genes and pathways involved in the regulation of *Drosophila* adult midgut homeostasis, we conducted a tissue-specific RNAi screen targeting the *Drosophila* kinome. We identified the membrane-associated kinase Gilgamesh (Gish)/Casein kinase 1 γ (CK1 γ) as essential for maintaining adult *Drosophila* midgut homeostasis by restricting aberrant ISC proliferation. We found that loss of Gish resulted in ectopic JNK pathway activation and excessive production of multiple cytokines and growth factors including ligands for EGFR, JAK-STAT, and Wg/Wnt pathways that fuel ISC proliferation. Mechanistically, we demonstrated that Gish restricts JNK pathway activity by phosphorylating and down-regulating Rho1, an upstream regulator of JNK signaling pathway (Neisch et al., 2010). Interestingly, we found that Gish expression is down-regulated in aging guts, leading to increased Rho1-JNK pathway activity and excessive ISC proliferation and that these aging phenotypes can be reversed by transient overexpression of Gish.

Results

A kinome screen identified Gish as an essential regulator of ISC proliferation and midgut homeostasis

To identify new regulators of midgut homeostasis, we performed a kinome screen in which UAS transgenic RNAi lines targeting individual kinases were expressed in adult guts using the progenitor (ISC + EB)-specific Gal4 driver *esg-Gal4* (Fig. 1 A), in conjunction with a temperature-sensitive Gal80 (referred to as *esg^{ts}* hereafter). This screen allowed us to identify Misshapen (Msn), a member of MAP4K family kinase, as a negative regulator of ISC proliferation (Li et al., 2014a, 2015). From the same screen, we found that expression of an RNAi line (BL #28066) targeting Gish/CK1 γ in progenitor cells (*esg^{ts}>Gish^{RNAi-1}* or *esg^{ts}>Gish^{RNAi}* for simplicity) resulted in increased ISC proliferation as indicated by an increase in the number of pH3-positive cells (Fig. 1, B–D). To rule out off-target effect, we examined two additional UAS-Gish-RNAi lines: *Gish^{RNAi-2}* (VDRC #106826) and *Gish^{RNAi-3}* (VDRC #26003) and obtained similar results (Fig. S1, A–E). Furthermore, coexpression of a UAS-Gish transgene suppressed ISC overproliferation caused by Gish RNAi (Fig. S1, F–I).

We further validated the Gish RNAi phenotype by mosaic analysis using the MARCM (mosaic analysis with a repressible cell marker) system in which both control and *gish* mutant clones were marked by GFP expression. Compared with the control clones, *gish* mutant clones exhibited increased clone size as indicated by the increased cell number per clone (Fig. 1, E–G). Of note, we only included ISC lineage clones in the R4 region of posterior midguts for quantification because of the regional difference in ISC proliferation rate (Buchon et al., 2013; Marianes and Spradling, 2013). Interestingly, there were more pH3-positive cells both inside and outside the *gish* mutant clones (Fig. 1, E, F, and H), suggesting that loss of Gish induced hyper-proliferation of ISCs likely through both cell-autonomous and non-cell-autonomous manners. Expression of a WT Gish (*Gish^{WT}*), but not its kinase-dead form (*Gish^{KD}*), rescued *gish* mutant phenotypes (Fig. S1, N–Q, S, and T). Deleting the C-terminal region of Gish (*Gish^{ΔC}*), which prevents Gish membrane association (Gault et al., 2012; Li et al., 2016),

also abolished its ability to suppress ISC overproliferation in *gish* mutant clones (Fig. S1, R–T). These observations suggest that Gish regulates ISC proliferation through its kinase activity and membrane association.

To determine in which cell types Gish exerts its function, we knocked down Gish in either ISCs, EBs, or ECs using the following cell type-specific Gal4 drivers: *DI-Gal4 Gal80^{ts}* (*DI^{ts}*) for ISC knockdown, *Su(H)-Gal4 Gal80^{ts}* (*Su(H)^{ts}*) for EB knockdown, and *Myo1A-Gal4 Gal80^{ts}* (*Myo1A^{ts}*) for EC knockdown, respectively (Fig. 1 A; Jiang et al., 2009; Tian et al., 2015, 2017). We found that Gish RNAi in any of these cell types resulted in increased ISC proliferation (Fig. 1, I–Q). In addition, coexpression of UAS-Gish transgene with UAS-Gish-RNAi in ECs suppressed ISC overproliferation (Fig. S1, J–M). These results suggest that Gish acts both cell autonomously and non-cell autonomously to restrict ISC proliferation.

Gish restricts the production of multiple cytokines and growth factors

The observation that loss of Gish can promote ISC proliferation in a non-cell-autonomous fashion suggests that Gish may regulate the production of niche signals that regulate ISC proliferation. Ligands of several signaling pathways including JAK-STAT, EGFR, and Wg/Wnt pathways have been implicated in the regulation of ISC proliferation during normal homeostasis and regeneration (Jiang et al., 2016). Indeed, we found that Gish RNAi in either progenitor cells (*esg^{ts}>Gish^{RNAi}*) or ECs (*Myo1A^{ts}>Gish^{RNAi}*) resulted in transcriptional up-regulation of multiple JAK-STAT pathway ligands (Upd, Upd2, and Upd3) and EGFR pathway ligands (Vn, Krn, and Spitz) as indicated by their increased mRNA levels determined by quantitative RT-PCR (RT-qPCR; Fig. 2 A). Gish RNAi in progenitor cells also up-regulated *wg* mRNA expression (Fig. 2 A). In addition, we found that Gish RNAi in either progenitor cells or ECs resulted in up-regulation of *upd3-lacZ* (Fig. 2, B–D). Of note, Gish RNAi in progenitor cells also up-regulated *upd3-lacZ* in many ECs adjacent to progenitor cell clusters (Fig. 2 C, arrows). This non-cell-autonomous up-regulation of *upd3-lacZ* is likely due to epithelial stress caused by ISC overproliferation (Patel et al., 2015). Consistent with the observed up-regulation of JAK-STAT pathway ligands, Gish RNAi in either progenitor cells or ECs resulted in elevated expression of JAK-STAT pathway target genes *10XStat-dGFP* and *Socs36E* (Fig. 2, A and F–I).

To determine whether the up-regulation of JAK-STAT and EGFR pathway activities contributed to the increased ISC proliferation in Gish RNAi midguts, we inactivated the JAK-STAT (*STAT^{RNAi}* or *Dome^{RNAi}*) or EGFR pathway (*EGFR^{RNAi}*) in either control or Gish-depleted progenitor cells. Although inactivation of the JAK-STAT or EGFR pathway alone did not affect ISC proliferation in the control guts under our experimental conditions, JAK-STAT or EGFR pathway inactivation suppressed ISC overproliferation caused by Gish RNAi (Fig. 2, J–R). Hence, Gish acts through the JAK-STAT and EGFR pathways to control ISC proliferation. Of note, *Dome^{RNAi}* did not completely suppress ISC overproliferation caused by *Gish^{RNAi}* as evident by residual clusters of pH3-positive cells (Fig. 2 Q), which is likely due to incomplete knockdown of *Dome*.

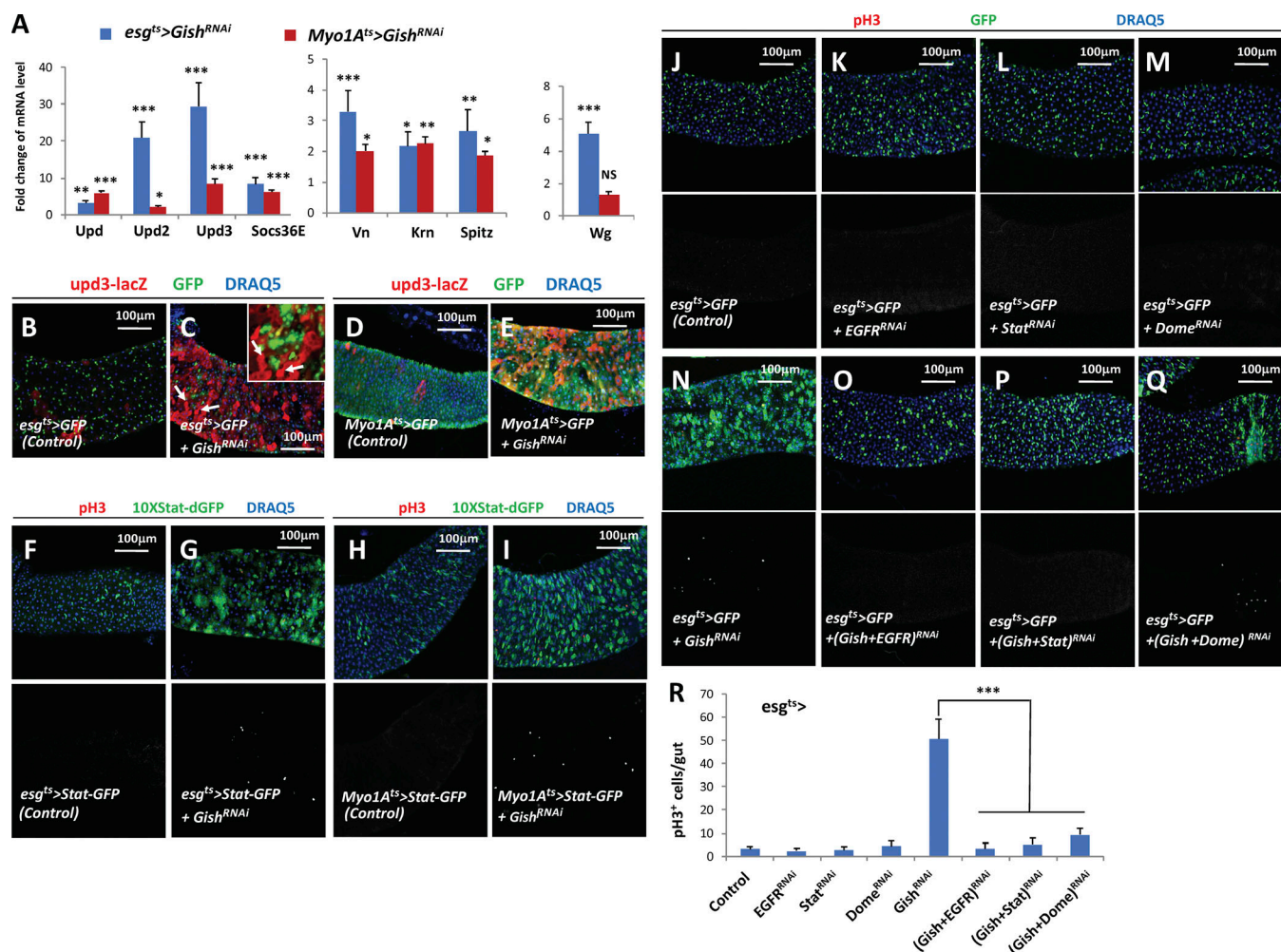


Figure 2. Loss of Gish increases the production of multiple growth factors. (A) mRNA levels of JAK-STAT, EGFR, and Wg pathway components in adult midguts of the indicated genotypes. Numbers on y axis indicate fold change normalized by control guts. Three independent experiments were performed. Data are mean ± SD. *P < 0.05, **P < 0.01, ***P < 0.001 (Student's t test). (B–I) Expression of *upd3-lacZ* (B–E) or *10XStat-dGFP* (F–I) in guts of the indicated genotypes. Inset in C shows an enlarged image of the area indicated by arrows. (J–Q) Adult midguts of the indicated genotypes were immunostained to show the expression of GFP and pH3. (R) Quantification of pH3⁺ cells in midguts of the indicated genotypes. Data are mean ± SD. ***P < 0.001 (Student's t test).

Loss of Gish leads to JNK pathway activation

The Hippo signaling pathway regulates ISC proliferation in both cell-autonomous and non-cell-autonomous manners (Karpowicz et al., 2010; Ren et al., 2010, 2013; Shaw et al., 2010; Staley and Irvine, 2010); however, inactivation of the Hippo pathway effector Yorkie (Yki) did not suppress the ISC overproliferation phenotype caused by Gish inactivation (Fig. S2), suggesting that Gish acts through other pathway(s) to restrict ISC proliferation.

Activation of the JNK pathway in either progenitor cells or ECs also resulted in ISC overproliferation (Biteau et al., 2008; Buchon et al., 2009; Jiang et al., 2009; Tian et al., 2015). In addition, JNK activation resulted in overproduction of ligands of the EGFR and JAK-STAT pathways (Jiang et al., 2009). Therefore, we examined whether loss of Gish resulted in activation of the JNK pathway. Indeed, we found that Gish RNAi in either progenitor cells or ECs resulted in up-regulation of a JNK pathway reporter gene *puc-lacZ* (*puc^{E96}*; Fig. 3, A–D), an enhancer trap line inserted in the *puckered* (*puc*) locus, which encodes a phosphatase that mediates negative

feedback regulation of the JNK pathway (Martín-Blanco et al., 1998). Careful examination of *puc-lacZ* expression in *esg^{ts}>GFP + Gish^{RNAi}* guts revealed that JNK pathway activation also occurred in ECs that are GFP negative (Fig. 3 B', arrows), which could explain the non-cell-autonomous activation of *upd3-lacZ* in *esg^{ts}>GFP + Gish^{RNAi}* guts (Fig. 2 C). However, Gish RNAi in progenitor cells for a shorter period of time (3 d at 29°C) did not significantly increase ISC proliferation but resulted in increased *puc-lacZ* expression primarily in GFP⁺ progenitor cells (Fig. S3, A–C), suggesting that cell-autonomous JNK activation could be a direct effect of Gish inactivation, while the non-cell-autonomous JNK activation observed in prolonged Gish RNAi guts is likely due to epithelial stress caused by ISC overproliferation similar to what has been described in a previous study (Patel et al., 2015). Consistent with Gish regulating JNK, Gish inactivation in wing imaginal discs also resulted in ectopic *puc-lacZ* expression (Fig. S3, E–G').

To determine whether activation of the JNK pathway is responsible for ISC overproliferation induced by loss of Gish, we

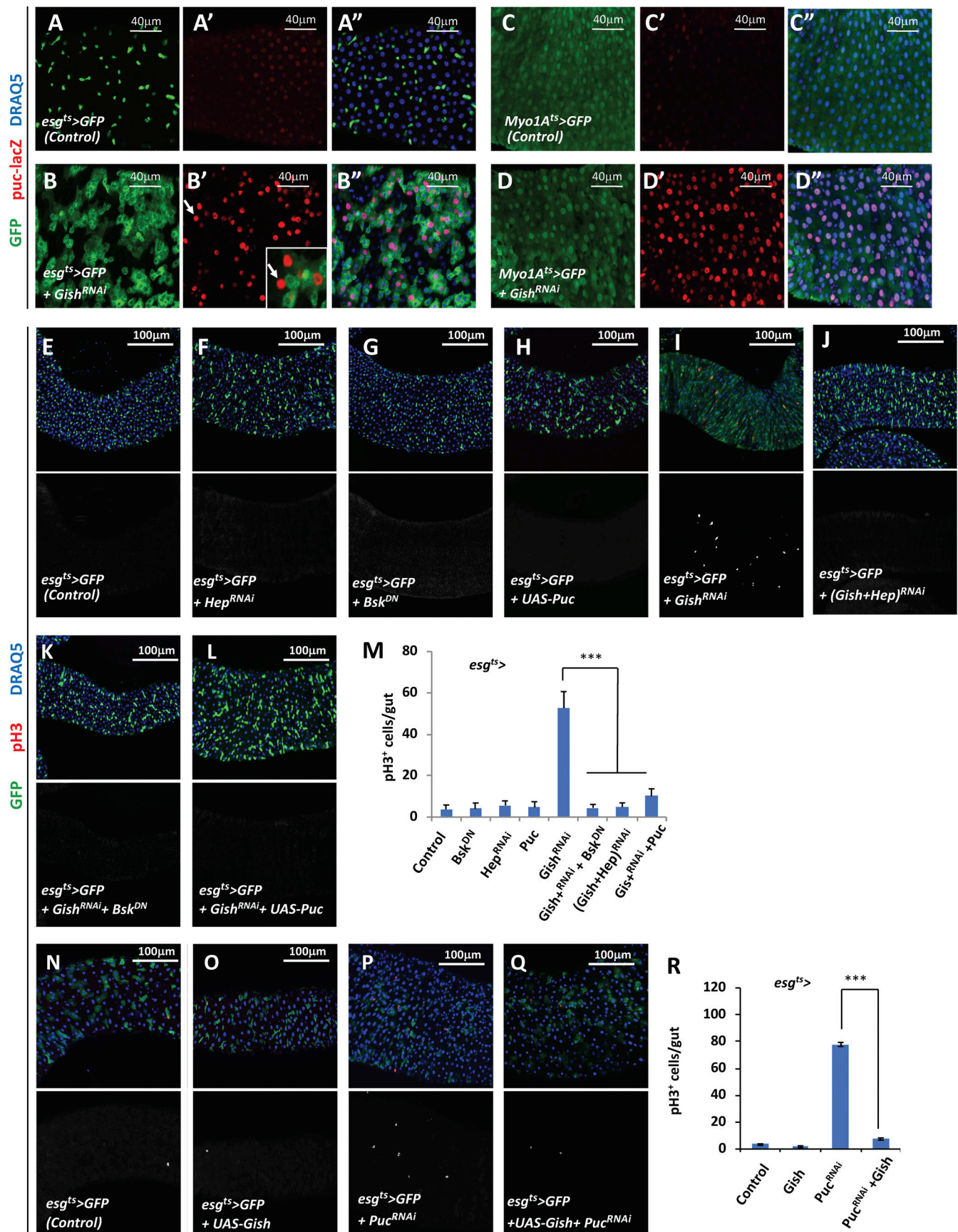


Figure 3. Gish regulates ISC proliferation by inhibiting JNK pathway. (A–D'') Expression of *puc-LacZ* (red), GFP (green) and DRAQ5 (blue) in control and Gish RNAi guts of the indicated genotypes. Inset in B' shows an enlarged image of the area indicated by the arrow. **(E–L)** Expression of pH3 (red), GFP (green), and DRAQ5 (blue) in adult midguts of the indicated genotypes. **(M)** Quantification of pH3⁺ cells in adult midguts of the indicated genotypes. *n* = 20 guts for each genotype. Data are mean ± SD. ****P* < 0.001 (Student's *t* test). **(N–Q)** Expression of pH3 (red), GFP (green), and DRAQ5 (blue) in adult midguts expressing *UAS-Gish* or *UAS-Puc-RNAi* either alone or in combination in progenitor cells for 3 d. **(R)** Quantification of pH3⁺ cells in adult midguts of the indicated genotypes. *n* = 20 guts for each genotype. Data are mean ± SD. ****P* < 0.001 (Student's *t* test).

inactivated the JNK pathway either by knockdown of the *Drosophila* JNK kinase Hemipterous (Hep) or by overexpression of a dominant-negative form of the *Drosophila* JNK Basket (Bsk), Bsk^{DN} (Weber et al., 2000), or the JNK pathway inhibitor Puc in progenitor cells of control guts or guts expressing *esg^{ts}>Gish^{RNAi}*. We found that inhibition of the JNK pathway blocked ISC overproliferation caused by Gish RNAi, although it did not affect the homeostatic ISC proliferation in the control guts (Fig. 3, E–M; and Fig. S4, A–E). On the other hand, Gish overexpression suppressed ISC overproliferation caused by ectopic JNK activation upon Puc RNAi (Fig. 3, N–R). In addition, overexpression of Bsk^{DN} partially inhibited the up-regulation of multiple cytokines and growth factors caused by Gish RNAi (Fig. S4, F and G). Taken together, these results demonstrated that Gish regulates ISC proliferation and tissue homeostasis by restricting aberrant JNK pathway activity.

Gish prevents ISC loss in response to JNK pathway activation

To further characterize the interaction between Gish and the JNK pathway, we inactivated Puc and Gish either alone or in combination by expressing the corresponding transgenic RNAi lines in midgut progenitor cells (*esg^{ts}*) for different periods of time (2, 5, and 12 d). Inactivation of either Gish or Puc alone resulted in a gradual increase in ISC proliferation over time (Fig. 4, A–C, E–G, I–K, and N). In addition, Gish RNAi and Puc RNAi had an additive effect on ISC proliferation when RNAi was conducted for 2 d (Fig. 4, D and N). However, when RNAi was conducted for 5 d, Gish RNAi appeared to reverse the effect on ISC proliferation caused by Puc RNAi because Gish and Puc double RNAi resulted in less pH3-positive cells compared with Puc RNAi alone (Fig. 4, E–H and N). The reduction of pH3-positive cells caused by Gish and Puc double RNAi was more striking after 12 d of RNAi (Fig. 4, I–L and N). In addition, *esg>GFP*-positive cells were diminished after double knockdown of Gish and Puc for 12 d (Fig. 4 L), suggesting that stem cells were lost. Expression of the cell death inhibitor Diap1 in Gish and Puc double RNAi progenitor cells partially restored *esg>GFP*-positive cells and pH3-positive cells (Fig. 4, M and N), suggesting that loss of stem cells in Gish and Puc double RNAi guts was largely due to apoptosis. Therefore, under the stress condition caused by excessive JNK pathway activation, Gish is required for ISC maintenance.

The genetic interaction between Gish and the JNK pathway in the regulation of cell survival was also observed in developing wings. For example, caspase-3 activation, which is a marker for apoptosis, was low in Gish RNAi wing discs and not detectable in *puc^{E96/+}* wing discs; however, Gish RNAi in *puc^{E96/+}* wing discs resulted in a dramatic activation of caspase-3, leading to a significant decrease of wing size (Fig. S3, D–K).

Because cell death caused by apoptosis in gut epithelium can stimulate ISC proliferation (Jiang et al., 2009), we asked whether cell death could contribute to ISC overproliferation caused by inactivation of Gish (Fig. S3 F). *UAS-Diap1* was coexpressed with *UAS-Gish-RNAi* in either progenitor cells (*esg^{ts}*) or EC (*Myo1A^{ts}*) to block apoptosis. Although overexpression of Diap1 in progenitor cells did not affect ISC overexpression caused by Gish RNAi in these cells (Fig. S4, H–L), coexpression of *UAS-Diap1* with *UAS-Gish-RNAi* in ECs partially suppressed the ectopic ISC proliferation (Fig. S4, M–Q), suggesting that activation of the apoptotic pathway may contribute to the nonautonomous effect of Gish RNAi on ISC proliferation.

Gish regulates JNK signaling through inhibiting Rho1

We next asked how Gish regulates JNK. The JNK pathway can be activated by Rho1, which activates the pathway through the *Drosophila* JNK kinase kinase (JNKKK) Slipper (Slpr) and Tak1 (Neisch et al., 2010). Interestingly, a previous study showed that mammalian RhoB, a homologue of Rho1, was phosphorylated by CK1 (Tillement et al., 2008). In addition, Gish was previously identified as a genetic modifier of Rho signaling (Gregory et al., 2007). These observations prompted us to determine whether Gish regulates the JNK pathway through Rho1. Indeed, inactivation of Rho1 by RNAi blocked ISC overproliferation in midguts where Gish was knocked down either in progenitor cells or ECs (Fig. 5, A–H). In addition, Rho1 RNAi blocked JNK pathway activation in Gish RNAi guts (Fig. 5, I–K). On the other hand, expression of a constitutively active form of Rho1 (Rho1^{V14}) induced JNK pathway activation (Fig. 5, L–O) and ISC overproliferation (Fig. 5, P–R). These results suggest that Gish acts through Rho1 to regulate the JNK pathway and gut homeostasis.

Gish-mediated phosphorylation regulates Rho1 protein stability

In addition to being regulated by GTP–GDP cycling through guanine nucleotide exchange factors, GTPase-activating proteins, and guanine nucleotide dissociation inhibitors, Rho GTPases can also be regulated by posttranslational modifications that alter their subcellular localization and protein stability (Hodge and Ridley, 2016). Using a transgene (*fTRG_3I*) that expresses GFP-tagged Rho1 (Rho1–GFP) under its endogenous promoter (Sarav et al., 2016), we found that Gish RNAi in either progenitor cells or ECs resulted in a cell-autonomous increase in Rho1–GFP protein levels (Fig. 6 A). Knockdown of Gish in wing imaginal discs also resulted in the up-regulation of Rho1–GFP (Fig. S5). By Western blot analysis, we found that Gish RNAi stabilized a Flag-tagged Rho1 (Fg-Rho1) expressed in S2 cells (Fig. 6 B). Treating cells with a proteasome inhibitor MG132 also stabilized Fg-Rho1 and eliminated the effect of Gish RNAi on Fg-Rho1

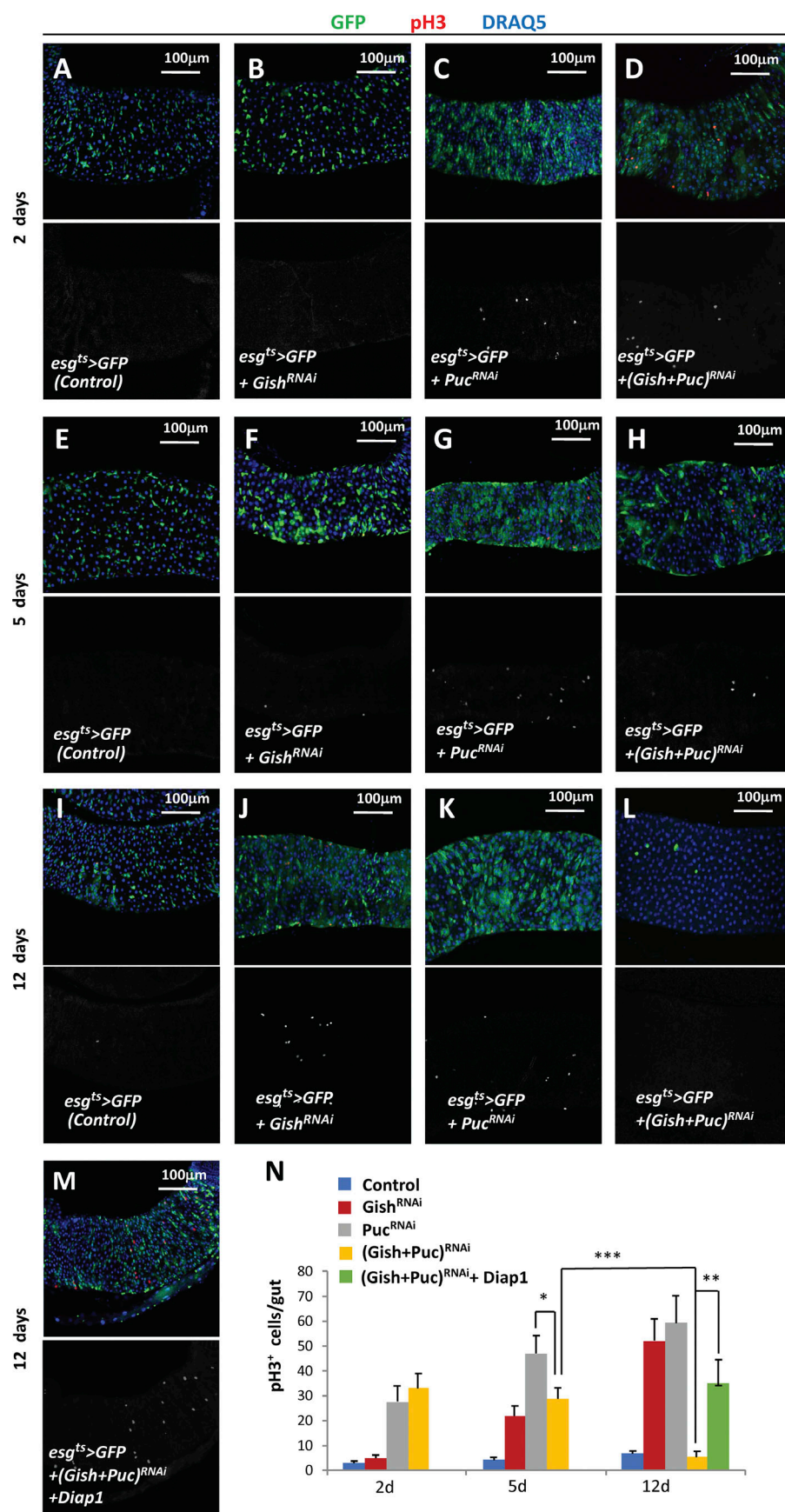


Figure 4. **Gish is required for stem cell maintenance under stress condition.** (A–M) Adult midguts expressing *esg^{ts}>GFP* (A, E, and I), *esg^{ts}>GFP* + *Gish^{RNAi}* (B, F, and J), *esg^{ts}>GFP* + *Puc^{RNAi}* (C, G, and K), *esg^{ts}>GFP* + *Gish^{RNAi}* + *Puc^{RNAi}* (D, H, and L), or *esg^{ts}>GFP* + *Gish^{RNAi}* + *Puc^{RNAi}* + *Diap1* for 2 d (A–D), 5 d (E–H), or 12 d (I–M) were immunostained for pH3 (red), GFP (green), and DRAQ5 (blue). (N) Quantification of pH3⁺ cells in midguts of the indicated genotypes. *n* = 20 guts for each genotype. Data are mean ± SD. **P* < 0.05, ***P* < 0.01, ****P* < 0.001 (Student's *t* test).

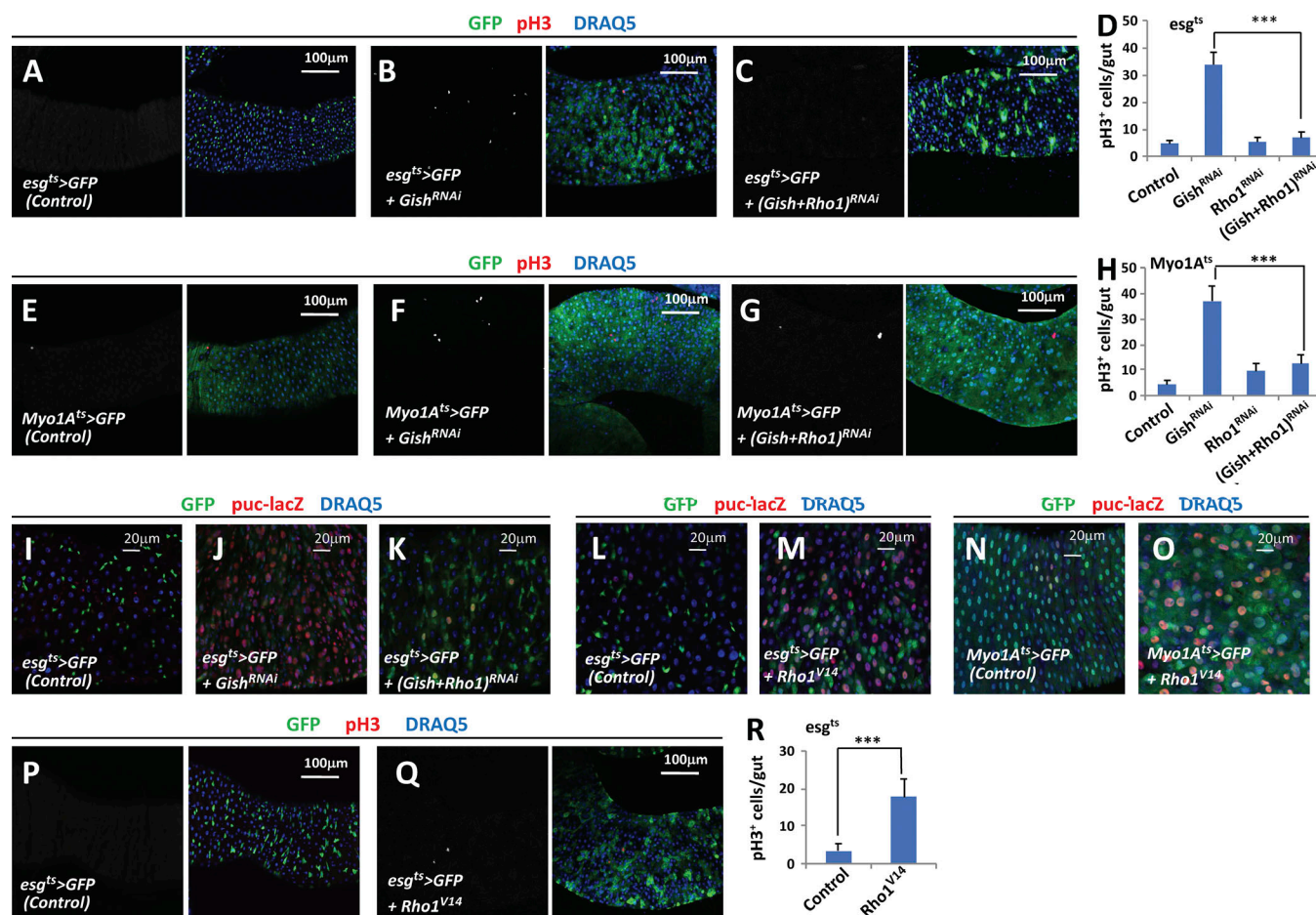


Figure 5. Gish regulates the JNK pathway through Rho1. (A–H) Adult midguts of the indicated genotypes were immunostained for pH3, GFP, and DRAQ5. Quantification of pH3⁺ cells in midguts of the corresponding genotype is shown in D and H. *n* = 18 guts for each genotype. Data are mean ± SD. ****P* < 0.001 (Student's *t* test). **(I–O)** Adult midguts of the indicated genotypes were immunostained for *puc-lacZ*, GFP, and DRAQ5. **(P and Q)** Adult midguts that expressed *esg^{ts}>GFP* (P) or *esg^{ts}>GFP + Rho1^{V14}* (Q) were immunostained for pH3, GFP, and DRAQ5. **(R)** Quantification of pH3⁺ cells in control or *Rho1^{V14}*-overexpressing guts. *n* = 18 guts for each genotype. Data are mean ± SD. ****P* < 0.001 (Student's *t* test).

protein stability (Fig. 6 B), suggesting that Gish may regulate Rho1 protein level through the ubiquitin/proteasome pathway. Indeed, Gish RNAi inhibited ubiquitination of Fg-Rho1 in S2 cells (Fig. 6 C).

We next asked whether Gish promoted Rho1 degradation by phosphorylating Rho1. CK1 phosphorylation sites usually contain an acidic residue or phosphorylated S/T at the -2, -3, or -4 position with the following consensus: D/E/(p)S/(p)T(p)[X1-3]S/T (underlined amino acid represents the CK1 phosphorylation site and X represents any amino acid; Knippschild et al., 2005). Inspection of the Rho1 amino acid sequence revealed a cluster of CK1 consensus sites including Ser88 and Ser91, which are conserved among the three mammalian Rho proteins: RhoA, RhoB, and RhoC (Fig. 6 D). Therefore, we generated a Rho1 variant with Ser88, Ser91, and an upstream Ser (Ser85) mutated to Ala (*Rho1^{SA}*). We found that both the steady-state level and half-life of Fg-Rho1^{SA} were increased compared with WT Fg-Rho1 in S2 cells (Fig. 6, E and F). In addition, Fg-Rho1^{SA} was no longer regulated by Gish since Gish RNAi did not increase the level of Fg-Rho1^{SA} (Fig. 6 F). Consistent with being more stable, Fg-Rho1^{SA} exhibited reduced ubiquitination compared with Fg-Rho1 (Fig. 6 G). In an in vitro

kinase assay, a recombinant CK1 kinase phosphorylated a GST fusion protein containing the Rho1 fragment from amino acid 65 to amino acid 111 (GST-Rho1₆₅₋₁₁₁) and this phosphorylation was abolished by the SA mutation (Fig. 6 H). These results suggest that phosphorylation of Rho1 by Gish promotes its degradation by the ubiquitin/proteasome pathway.

To determine the physiological function of CK1-mediated phosphorylation of Rho1, we generated transgenic flies expressing either *UAS-Fg-Rho1* or *UAS-Fg-Rho1^{SA}* inserted into the same genetic locus using the phiC31 integrase system. By Western blot analysis, we confirmed that Fg-Rho1^{SA} was more stable than Fg-Rho1 when expressed in adult midguts (Fig. 6 I). When expressed in progenitor cells using *esg^{ts}*, Fg-Rho1^{SA} drove more ISC proliferation than Fg-Rho1 (Fig. 6, J and K). These results suggest that CK1-mediated phosphorylation restricts Rho1 activity by promoting its degradation to maintain midgut homeostasis.

Gish is down-regulated in aging guts

Because Gish inactivation resulted in increased ISC proliferation and JNK pathway activation—phenotypes also observed in aging guts (Biteau et al., 2008; Li et al., 2014b)—we went on to determine

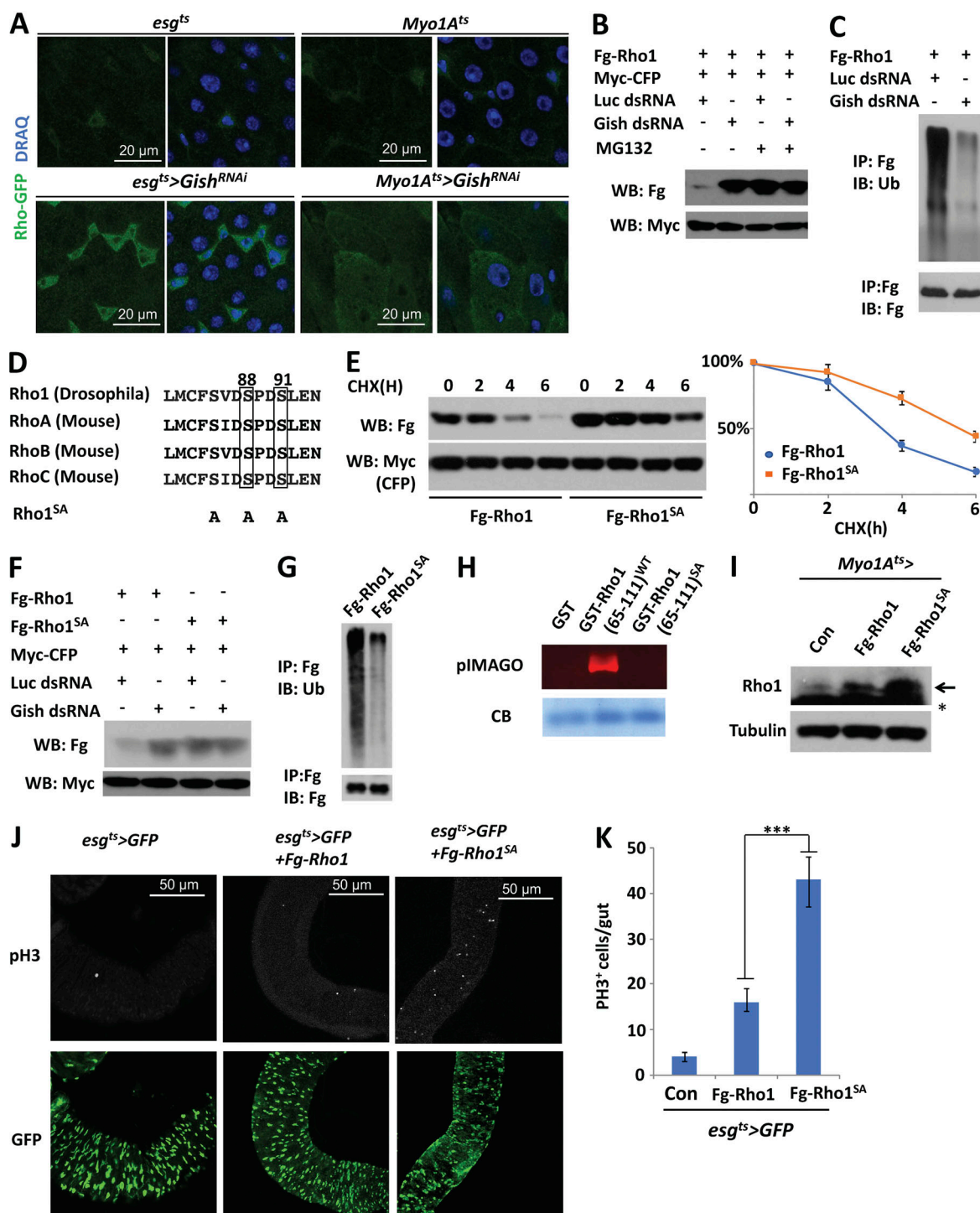


Figure 6. Gish phosphorylates Rho1 to promote its degradation. (A) Rho-GFP in adult midguts of the indicated genotypes. **(B)** Western blot analysis of Fg-Rho1 transfected into S2 cells treated with control (Luc) or Gish dsRNA. Cells were treated with or without MG132 for 4 h before harvesting. Myc-CFP was cotransfected as internal control. **(C)** Ubiquitination of Fg-Rho1 transfected into S2 cells treated with control (Luc) or Gish dsRNA. Cells were treated with MG132 for 4 h before harvesting. **(D)** Sequence alignment of *Drosophila* Rho1 and mouse Rho family members with the putative CK1 sites highlighted. **(E)** Western blot analysis and quantification of Fg-Rho1 and Fg-Rho1^{SA} transfected into S2 cells at the indicated time point following cycloheximide (CHX) treatment. Myc-CFP was used as loading control. **(F)** Western blot analysis of Fg-Rho1 and Fg-Rho1^{SA} transfected into S2 cells treated with control (Luc) or Gish dsRNA. Myc-CFP was cotransfected as internal control. **(G)** Ubiquitination of Fg-Rho1 and Fg-Rho1^{SA} transfected into S2 cells. Cells were treated with MG132 for 4 h before harvesting. **(H)** In vitro kinase assay of the indicated GST-Rho1 fusion proteins and recombinant CK1 using the pIMAGO kit. Coomassie blue (CB) staining showed equal amounts of GST fusion proteins. **(I)** Western blot analysis of Rho1 in adult guts of the indicated genotypes. Arrow and asterisk indicate Rho1 and a nonspecific band, respectively. **(J and K)** Adult midguts of the indicated genotypes were immunostained for pH3 and GFP (J). Quantification of pH3⁺ cells in midguts of the corresponding genotype is shown in K. *n* = 20 guts for each genotype. Data are mean \pm SD from three independent experiments. ****P* < 0.001 (Student's *t* test). IB, immunoblot; IP, immunoprecipitation; WB, Western blot.

whether Gish activity changes during aging. By RT-qPCR and immunostaining, we found that Gish mRNA and protein levels decreased in old guts (20 and 30 d) compared with young guts (10 d; Fig. 7, A–D). Consistent with the reduction of Gish expression in old guts, the level of Rho1-GFP increased in old guts compared with young guts (Fig. 7, E–F). In addition, Gish overexpression suppressed the up-regulation of Rho1-GFP in the aging guts (Fig. 7, G and G'). These observations raise an interesting possibility that a decline of Gish activity may contribute to the aging phenotypes in the guts. To test this hypothesis, we aged *esg^{ts}>GFP* or *esg^{ts}>GFP* + Gish flies for 45 d at 18°C and then shifted to 29°C to induce Gish transgene expression. Compared with young guts (*esg^{ts}>GFP*; 10 d at 18°C), 50-d-old guts (*esg^{ts}>GFP*; 45 d at 18°C and 5 d at 29°C) exhibited increased JNK pathway activity and elevated ISC proliferation, as indicated by increased *puc-lacZ* expression and pH3⁺ cells, respectively (Fig. 7, H–I', K–L', and N). These aging-related phenotypes were suppressed by transgenic expression of Gish in the old guts (*esg^{ts}>GFP* + Gish; 45 d at 18°C and 5 d at 29°C; Fig. 7, J–J', M, and N). Of note, Gish overexpression in ISCs/EBs not only suppressed *puc-lacZ* in progenitors but also in ECs (Fig. 7, I'–J', insets). The non-cell-autonomous suppression of *puc-lacZ* in ECs is likely due to the reduced ISC proliferation in these guts. Hence, down-regulation of Gish may contribute to the increased JNK pathway activation and elevated ISC proliferation in aging guts.

Discussion

Adult stem cells are essential for tissue homeostasis and regeneration, and their activity needs to be tightly controlled in order to maintain the normal cellular architecture and physiological function of adult organs. The JNK pathway plays a pivotal role in the *Drosophila* midgut homeostasis and injury response. In addition, JNK pathway activity is elevated in aging guts, leading to aberrant stem cell proliferation and loss of tissue homeostasis. How the JNK pathway is kept in check during gut homeostasis and aging is not well understood. Here, we provide both genetic and biochemical evidence that the membrane-associated kinase Gish/CK1 γ restricts JNK pathway activity by phosphorylating and destabilizing Rho1, an upstream activator of the JNK pathway (Fig. 8). This regulatory pathway is critical for the maintenance of midgut homeostasis as loss of Gish results in elevated JNK pathway activity and ISC proliferation. Interestingly, Gish expression in the midgut declines with aging, which may contribute to the elevated JNK pathway activity and ISC overproliferation in old guts. In support of this notion, we found that transgenic expression of Gish in old guts could restore JNK pathway activity and ISC proliferation to homeostatic levels. How Gish expression is down-regulated in aging guts remains an open question, but it appears to occur at the level of transcription, although we cannot rule out the possibility that posttranscriptional regulation may also occur. The precise mechanism awaits further investigation.

Prolonged activation of JNK can induce apoptosis in both *Drosophila* and mammalian cells (Moreno et al., 2002; Liu and Lin, 2005). As a negative regulator of JNK pathway activity, Gish synergizes with Puc, another JNK pathway inhibitor, to protect ISCs from undergoing apoptosis; thus, it may play a role in stem cell maintenance under stress condition. The synergistic interaction

between Gish and Puc is not restricted to ISCs but also occurs in other tissues. For example, in wing imaginal discs, depletion of Gish only resulted in low levels of apoptosis; however, removal of one copy of *puc* (*puc^{E96/+}*) in Gish-depleted wing discs (*MS>Gish^{RNAi}, puc^{E96/+}*) resulted in massive cell death, leading to the formation of small wings (Fig. S5). The increased apoptosis in *MS>Gish^{RNAi}, puc^{E96/+}* appeared to mirror the dramatic activation of the JNK pathway. Hence, the cell- and tissue-protective function of Gish could simply be attributed to its role in suppressing JNK signaling. However, it remains possible that other pathways downstream of Rho1 and/or Gish may contribute to the induction of apoptosis in Gish and Puc double-deleted cells in parallel to heightened JNK pathway activity.

Although mainly regulated by GTP–GDP cycling, Rho GTPases can also be regulated by posttranslational modifications such as phosphorylation that control their subcellular localization, stability, and complex formation (Hodge and Ridley, 2016). For example, a previous study showed that Erk2-mediated phosphorylation of RhoA targeted it for ubiquitin/proteasome-mediated degradation in cultured epithelial cells (Wei et al., 2013). However, the phosphorylation site(s) on RhoA that regulates its stability remained unidentified, and the physiological role of Erk2-mediated phosphorylation of RhoA was not determined. Here, we provided both genetic and biochemical evidence that Gish phosphorylates a cluster of sites in the N-terminal region of Rho1, which targets Rho1 for ubiquitination, followed by proteasome-mediated degradation. Gish-mediated down-regulation of Rho1 restricts JNK pathway activity, which is critical for adult *Drosophila* midgut homeostasis. How Rho1 inhibits JNK pathway remains an open question. A previous study revealed that Rho1 physically interacts with Slpr/JNKKK regardless of its GDP/GTP binding state and that Rho1 promotes Slpr cortical localization (Neisch et al., 2010). Therefore, it is possible that plasma membrane-associated Rho1 promotes JNK pathway activation by increasing the local concentration of Slpr/JNKKK at the plasma membrane. The precise biochemical mechanism by which Rho1 activates Slpr/JNKKK awaits further investigation.

Rho GTPases shuttle between plasma membrane and cytoplasm with GTP-bound active forms associated with membrane (Hodge and Ridley, 2016). Gish/CK1 γ belongs to the CK1 family kinases. Unlike other family members that are located mainly in the cytoplasm, Gish/CK1 γ is associated with plasma membrane through its C-terminal lipid modification. We demonstrated that the function of Gish in restricting ISC overproliferation depended on its kinase activity and membrane association (Fig. S1), suggesting that Gish may phosphorylate plasma membrane-associated Rho1 to prevent its aberrant accumulation at the plasma membrane where it can activate the JNK pathway (Neisch et al., 2010). This may explain why the role of Gish/CK1 γ cannot be replaced by other CK1 family members. Since the CK1 phosphorylation sites on Rho1 are also found in all members of mammalian Rho GTPase, we speculate that CK1 γ may play a conserved role in the regulation of Rho GTPase activity. Future study is needed to determine whether CK1 γ regulates Rho GTPase activity and whether such regulation plays a role in development, tissue homeostasis, and aging in mammals.

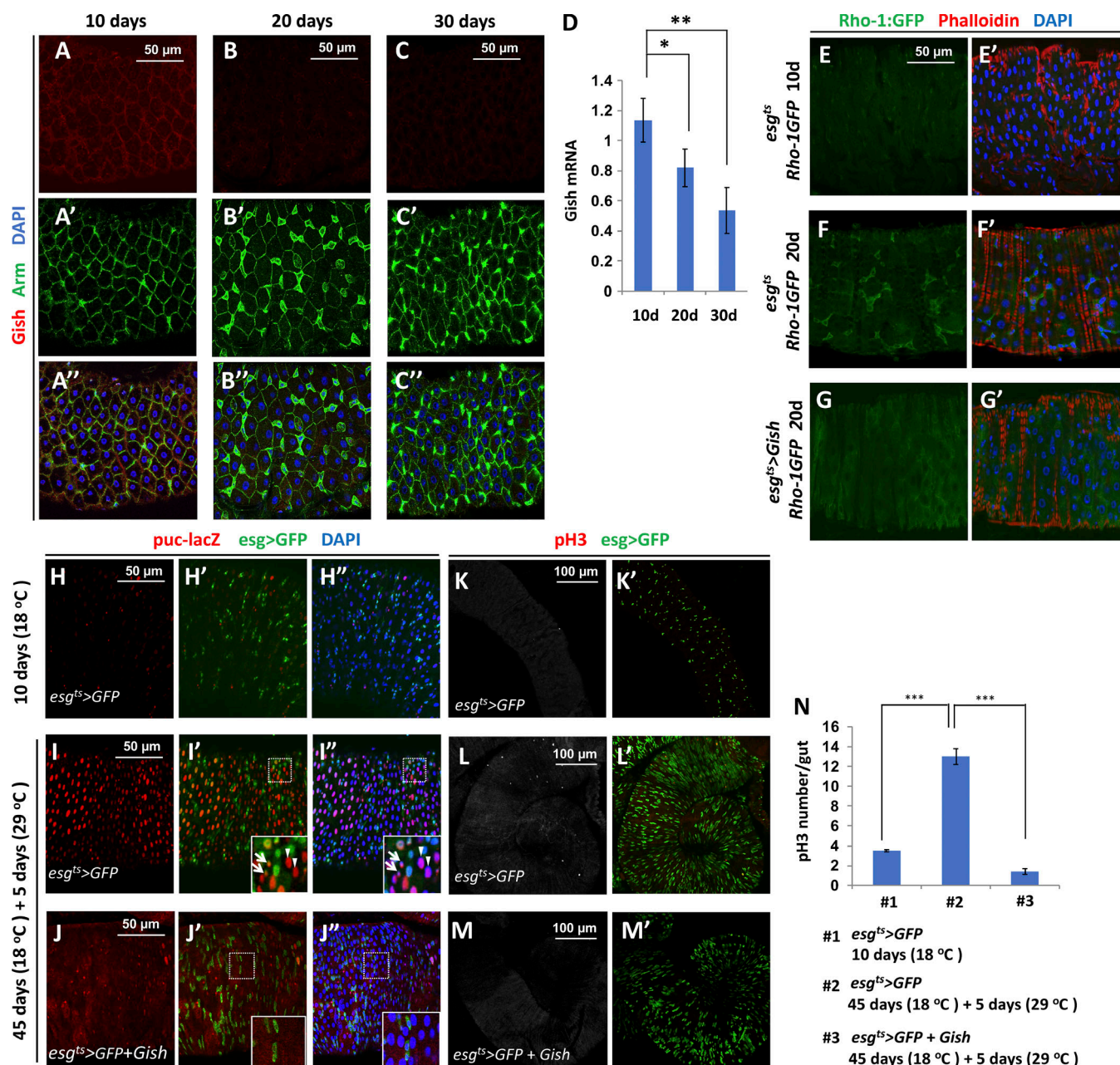


Figure 7. Gish is down-regulated in aging guts. (A–D) Gish immunostaining (A–C) or mRNA level measured by RT-qPCR (D) in adult midguts of the indicated age. Arm staining was used as an internal control for immunostaining. Data are mean ± SD from three independent experiments. * $P < 0.05$, ** $P < 0.01$ (Student's t test). **(E–G)** Rho1-GFP expression in young (E and E') and old (F–G) guts with (G and G') or without (E–F') Gish overexpression. Phalloidin staining was used as an internal control. **(H–J)** *puc-lacZ* expression in 10-d-old (H–H') or 50-d-old (I–I') guts without (I–I') or with (J–J') transgenic *gish* expression for 5 d. Insets show enlarged images of the indicated areas. Arrows and arrowheads indicate increased *puc-lacZ* expression in progenitor cells and ECs, respectively. **(K–M)** pH3 staining in 10-d-old (K and K') or 50-d-old (L–L') guts without (L and L') or with 5-d transgenic expression of Gish (M and M'). **(N)** Quantification of pH3⁺ cells in midguts of indicated samples. $n = 12$ guts for each sample set. Data are mean ± SD from three independent experiments. *** $P < 0.001$ (Student's t test).

Materials and methods

Drosophila genetics and transgenes

The following fly strains were used: *gish*^{KG03891} contains a P element inserted into the *gish* locus (BL #13263); *UAS-Gish-RNAi* (VDR #106826, VDR #26003, BL #28066); *UAS-EGFR-RNAi* (VDR #43267); *UAS-Stat-RNAi* (VDR #43866); *UAS-Dome-RNAi* (BL #34618); *UAS-Hep-RNAi* (BL #11790); *UAS-Puc-RNAi* (VDR

#3018); *UAS-Rho-RNAi* (BL #27727); *UAS-Yki-RNAi* (Zhang et al., 2008); *fTRG_31* expresses Rho1-GFP under its endogenous promoter (VDR #318439); *UAS-Myc-Gish* (BL #41764), *UAS-Myc-Gish^{KD}* (BL #41766), and *UAS-Myc-Gish^{ΔC}* (BL #41769) express WT, kinase-dead, and ΔC forms of Gish, respectively; *UAS-Puc* expresses a full-length WT Puc (FlyORF F001556); *UAS-BSK^{DN}* expresses a dominant-negative form of

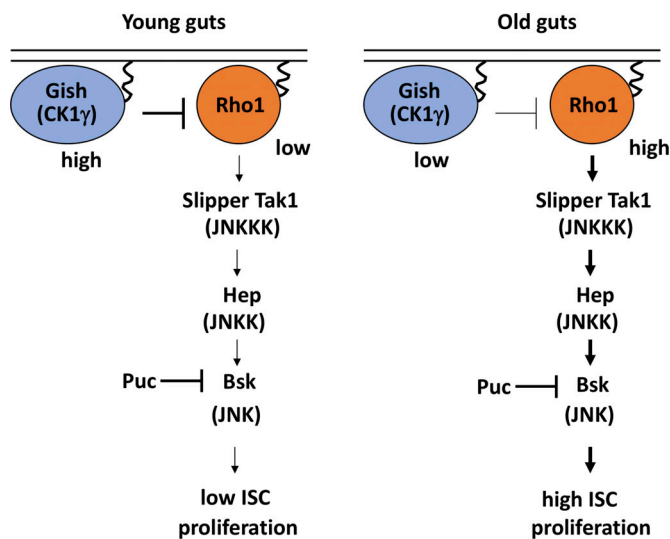


Figure 8. Gish maintains ISC quiescence and tissue homeostasis by restricting JNK pathway activation. In young guts, Gish expression is high. Membrane-associated Gish phosphorylates Rho1 to promote its degradation, which is required for keeping JNK pathway activity and ISC proliferation low. In old guts, Gish expression is down-regulated, leading to elevated Rho1–JNK pathway activity and increased ISC proliferation.

BSK (BL #6409); *UAS-Rho1^{V14}* expresses a constitutively active form of Rho1 (BL #8144); *10XStat-dGFP* is a JAK–STAT pathway reporter gene that contains 10 copies of STAT-binding sites fused to a GFP coding sequence (Bach et al., 2007). *esg-Gal4* (a GAL4 enhancer trap insertion in the *esg* locus); *Myo1A-Gal4* (a GAL4 enhancer trap insertion in the *Myosin 1A* locus); *Su(H)-Gal4* contains three copies of the GRH-binding elements and two copies of Su(H) binding sites fused to GAL4 coding sequence; *Dl-Gal4* has a GAL4 coding sequence inserted in the *Dl* locus (Zeng et al., 2010); *hh-Gal4* has a GAL4 coding sequence inserted in the *hh* locus (Cho et al., 2018); *MS1096* is a wing-specific Gal4 driver (Wang et al., 1999); *tub-Gal80^{ts}* expresses a temperature-sensitive Gal80 under the control of tubulin promoter (McGuire et al., 2004); *puc-lacZ* (*puc^{E69}*, a *lacZ* enhancer trap at the *puc* locus). To generate *UAS-Flag-Gish*, *UAS-Flag-Rho1*, and *UAS-Flag-Rho1^{SA}* constructs, DNA fragments encoding Gish, Rho1 with WT or mutated CK1 sites were amplified by PCR and inserted into the *Flag-pUAST* vector (Tong and Jiang, 2007). Transgenic flies carrying *UAS-Flag-Gish*, *UAS-Flag-Rho1*, and *UAS-Flag-Rho1^{SA}* were generated by P element-mediated transformation using the phiC31 integration system (Bischof et al., 2007).

Clone induction and transgene activation by Gal4 in conjunction with Gal80^{ts}

Mutant clones for *gish^{KG03891}* were generated using the MARCM system (Lee and Luo, 2001), with the following stock: *hs-flp UAS-GFP; tub-Gal4; FRT82B tub-Gal80/FRT82B gish^{KG03891}*. To induce MARCM clones, fly stocks were crossed and cultured at 18°C, and 3–5-d-old F1 adult flies with the appropriate genotypes were subjected to heat shock in empty vials for 1 h in a 37°C water bath. After clone induction, flies

were transferred to new cornmeal food every 2 d and raised at 18 or 25°C for 7–10 d before dissection. For experiments involving *Gal4/Gal80^{ts}*, crosses were set up and cultured at 18°C to restrict Gal4 activity. 2–3-d-old F1 adult flies were then shifted to 29°C to inactivate Gal80^{ts}, allowing Gal4 to activate UAS transgenes.

Immunostaining and microscopy

Female flies were used for gut immunostaining in all experiments. The entire gastrointestinal tracts were dissected out and fixed in 1× PBS plus 8% EM-grade paraformaldehyde (Polysciences) for 2 h. Samples were washed and incubated with primary and secondary antibodies in a solution containing 1× PBS, 0.5% BSA, and 0.1% Triton X-100. The following primary antibodies were used: rabbit anti-Gish (Tan et al., 2010), 1:500; mouse anti-Delta (Developmental Studies Hybridoma Bank), 1:100; rabbit anti-lacZ (Cell Signaling Technology), 1:1,000; mouse anti-pH3 (Millipore), 1:2,000; goat anti-GFP (Abcam), 1:500; rabbit anti-cleaved caspase-3, 5A1E (Cell Signaling Technology), 1:1,000; and DRAQ5 (Cell Signaling Technology), 1:5,000. Alexa Fluor-conjugated secondary antibodies were used at 1:400 (Jackson ImmunoResearch and Invitrogen). Guts were mounted in 70% glycerol and imaged with an inverted confocal microscope (LSM 710; Zeiss) using 10×, 20×, and 40× oil objectives (imaging medium: Immersol 518F; Zeiss). Imaging acquisition was performed at room temperature with LSM Image Browser (Zeiss), and image processing was done in Adobe Photoshop CC.

RT-qPCR

Total RNA was extracted from 15 female guts using RNeasy Plus Mini Kit (#74134; Qiagen), and cDNA was synthesized using the iScript cDNA synthesis kit (Bio-Rad). RT-qPCR was performed using iQ SYBR Green System (Bio-Rad). RT-qPCR was performed in triplicate on each of three independent biological replicates. Primer sequences used were as follows: *upd*: forward primer, 5'-CCACGTAAGTTTGCATGTTG-3'; reverse primer, 5'-CTAAACAGTAGCCAGGACTC-3'; *upd2*: forward primer, 5'-ACTGTTGCA TGTGGATGCTG-3'; reverse primer, 5'-CAGCCAAGGACGAGT TATCA-3'; *upd3*: forward primer, 5'-GAGCACCAAGACTCTGGA CA-3'; reverse primer, 5'-CCAGTGCAACTTGATGTTGC-3'; *Socs36E*: forward primer, 5'-CAGTCAGCAATATGTTGTGC-3'; reverse primer, 5'-ACTTGCAGCATCGTCGCTTC-3'; *Vn*: forward primer, 5'-TCACACATTTAGTGGTGGAAAG-3'; reverse primer, 5'-TTGTGATGCTTGAATTGGTAA-3'; *Spi*: forward primer, 5'-CGCCCAAGAATGAAAGAGAG-3'; reverse primer, 5'-AGGTAT GCTGCTGGTGGAAAC-3'; *Krn*: forward primer, 5'-CGTGTGTTGG CAACAACAAGT-3'; reverse primer, 5'-TGTGGCAATGCAGTT TAAGG-3'; *Wg*: forward primer, 5'-GATTATCCGCAGTCTGG TC-3'; reverse primer, 5'-CTATTATGCTTGCGTCCCTG-3'; and *Gish*: forward primer, 5'-ATCGGTGATACGAAACGAGCAA-3'; reverse primer, 5'-CAAACCTCTCCGGATGTCCATCA-3'.

Cell culture, transfection, and RNAi

S2 cells were cultured in Schneider's *Drosophila* medium (Life Technologies) with 10% FBS (GE Healthcare), penicillin (100

U/ml; Life Technologies), and streptomycin (100 mg/ml; Life Technologies) at 24°C. Transfection of S2 cells was performed using Calcium Phosphate Transfection Kit (Specialty Media) following the manufacturer's instructions. *UAS-Flag-Rho/UAS-Flag-Rho^{SA}* was cotransfected with actin-Gal4 to express the Flag-Rho/Rho^{SA} in S2 cells. Double-stranded (ds) RNA was generated using the MEGAscript High Yield Transcription Kit (#AM1334; Ambion) according to the manufacturer's instructions. dsRNA targeting the coding sequence of luciferase was used as a control. The following primers were used for generating the dsRNA targeting Gish: 5'-GAATTAATACGACTCACTATAGGGAGAGGCAGAACGTCAACAAAACGT-3' and 5'-GAATTAATACGACTCACTATAGGGAGATTTTGGCGCGTCGATTCTT-3'.

Immunoprecipitation and Western blot analysis

Cell lysates were precleared by incubation with protein A-Sepharose beads for 1 h or overnight at 4°C. After removal of the protein A beads by centrifugation, the cleared lysates were incubated with antibody for 2–4 h at 4°C. The immune complexes were collected by incubation with protein A-Sepharose beads for 1 h at 4°C, followed by centrifugation. The immunoprecipitates were then washed three times for 10 min each with lysis buffer. Samples were then heated for 5 min at 100°C in SDS loading buffer. Samples were separated on 10% polyacrylamide gel and transferred to nitrocellulose membranes (Life Technologies, Thermo Fisher Scientific). After blocking with 5% BSA in TBS with 0.5% Tween 20 for 1 h, the membranes were probed with the corresponding antibodies overnight. Bound antibodies were visualized by ECL (EMD Millipore or Pierce, Thermo Fisher Scientific) using HRP-conjugated antibodies.

Ubiquitination assay

S2 cells transfected with Flag-Rho constructs in the absence or presence of Gish dsRNA were treated with 50 μM MG132 (Calbiochem) for 4 h to inhibit proteasome-mediated degradation before harvest. Cells were lysed in 100 μl of denaturing buffer (1% SDS, 50 mM Tris, pH 7.5, 0.5 mM EDTA, and 1 mM DTT). After incubation for 1 min at 100°C, the lysates were diluted 10-fold with lysis buffer and then subjected to immunoprecipitation and Western blot analysis.

In vitro kinase assay

In vitro kinase assay was performed by incubating 25 μl of reaction mixtures containing 150 mM Tris-HCl, pH 7.5, 0.2 mM Mg²⁺/ATP, and 1 μg of purified GST-Rho1 fusion proteins, together with 1 μl of recombinant CK1δ (New England Biolabs) at 30°C for 1.5 h. The reaction was terminated by adding 2× SDS loading buffer. The resultant samples were load on SDS-PAGE and subjected to pIMAGO phosphoprotein detection kit with Alexa Fluor 680 (Sigma-Aldrich).

Genotypes for figures and supplemental figures

Fig. 1

(B) w; *esg-Gal4 tub-Gal80^{ts} UAS-GFP/+*. (C) w; *esg-Gal4 tub-Gal80^{ts} UAS-GFP/UAS-Gish-RNAi¹⁰⁶⁸²⁶*. (E) *yw UAS-GFP hsf1p/+*; *tub-Gal4/+*; *FRT82B tub-Gal80/FRT82B*. (F) *yw UAS-GFP hsf1p/+*; *tub-Gal4/+*; *FRT82B tub-Gal80/FRT82B gish^{KGO3891}*. (I) *DI-Gal4*

tub-Gal80^{ts} UAS-GFP/+. (J) *DI-Gal4 tub-Gal80^{ts} UAS-GFP/UAS-gish-RNAi¹⁰⁶⁸²⁶*. (L) *Su(H)-Gal4 tub-Gal80^{ts} UAS-GFP/+*. (M) *Su(H)-Gal4 tub-Gal80^{ts} UAS-GFP/UAS-Gish-RNAi¹⁰⁶⁸²⁶*. (O) w; *Myo1A-Gal4 tub-Gal80^{ts} UAS-GFP/+*. (P) w; *Myo1A-Gal4 tub-Gal80^{ts} UAS-GFP/UAS-Gish-RNAi¹⁰⁶⁸²⁶*.

Fig. 2

(B) w; *esg-Gal4 tub-Gal80^{ts} UAS-GFP/+*; *upd3-lacZ*. (C) w; *esg-Gal4 tub-Gal80^{ts} UAS-GFP/UAS-Gish-RNAi¹⁰⁶⁸²⁶*; *upd3-lacZ*. (D) w; *Myo1A-Gal4 tub-Gal80^{ts} UAS-GFP/+*; *upd3-lacZ*. (E) w; *Myo1A-Gal4 tub-Gal80^{ts} UAS-GFP/+*; *UAS-Gish-RNAi¹⁰⁶⁸²⁶*; *upd3-lacZ*. (F) w; *esg-Gal4 tub-Gal80^{ts}/UAS-10XStat-dGFP*. (G) w; *esg-Gal4 tub-Gal80^{ts}/UAS-10XStat-dGFP*; *UAS-Gish-RNAi²⁸⁰⁶⁶*. (H) w; *Myo1A-Gal4 tub-Gal80^{ts}/UAS-10XStat-dGFP*. (I) w; *Myo1A-Gal4 tub-Gal80^{ts}/UAS-10XStat-dGFP*; *UAS-gish-RNAi²⁸⁰⁶⁶*. (J) w; *esg-Gal4 tub-Gal80^{ts} UAS-GFP/+*. (K) w; *esg-Gal4 tub-Gal80^{ts} UAS-GFP/+*; *UAS-EGFR-RNAi*. (L) w; *esg-Gal4 tub-Gal80^{ts} UAS-GFP/+*; *UAS-Stat-RNAi*. (M) w; *esg-Gal4 tub-Gal80^{ts} UAS-GFP/+*; *UAS-Dome-RNAi*. (N) w; *esg-Gal4 tub-Gal80^{ts} UAS-GFP/+*; *UAS-Gish-RNAi²⁸⁰⁶⁶*. (O) w; *esg-Gal4 tub-Gal80^{ts} UAS-GFP/+*; *UAS-gish-RNAi²⁸⁰⁶⁶/UAS-EGFR-RNAi*. (P) w; *esg-Gal4 tub-Gal80^{ts} UAS-GFP/+*; *UAS-Gish-RNAi²⁸⁰⁶⁶/UAS-Stat-RNAi*. (Q) w; *esg-Gal4 tub-Gal80^{ts} UAS-GFP/+*; *UAS-Gish-RNAi²⁸⁰⁶⁶/UAS-Dome-RNAi*.

Fig. 3

(A) w; *esg-Gal4 tub-Gal80^{ts} UAS-GFP/+*; *puc-lacZ*. (B) w; *esg-Gal4 tub-Gal80^{ts} UAS-GFP/UAS-gish-RNAi¹⁰⁶⁸²⁶*; *puc-lacZ*. (C) w; *Myo1A-Gal4 tub-Gal80^{ts} UAS-GFP/+*; *puc-lacZ*. (D) w; *Myo1A-Gal4 tub-Gal80^{ts} UAS-GFP/UAS-gish-RNAi¹⁰⁶⁸²⁶*; *puc-lacZ*. (E) w; *esg-Gal4 tub-Gal80^{ts} UAS-GFP/+*. (F) w; *esg-Gal4 tub-Gal80^{ts} UAS-GFP/+*; *UAS-Hep-RNAi*. (G) *UAS-Bsk^{DN}*; *esg-Gal4 tub-Gal80^{ts} UAS-GFP/+*. (H) w; *esg-Gal4 tub-Gal80^{ts} UAS-GFP/+*; *UAS-Puc*. (I) w; *esg-Gal4 tub-Gal80^{ts} UAS-GFP/+*; *UAS-gish-RNAi²⁸⁰⁶⁶*. (J) w; *esg-Gal4 tub-Gal80^{ts} UAS-GFP/+*; *UAS-gish-RNAi²⁸⁰⁶⁶/Hep^{RNAi}*. (K) *UAS-Bsk^{DN}*; *esg-Gal4 tub-Gal80^{ts} UAS-GFP/+*; *UAS-gish-RNAi²⁸⁰⁶⁶*. (L) w; *esg-Gal4 tub-Gal80^{ts} UAS-GFP/UAS-Puc*; *UAS-gish-RNAi²⁸⁰⁶⁶*. (N) w; *esg-Gal4 tub-Gal80^{ts} UAS-GFP*. (O) w; *esg-Gal4 tub-Gal80^{ts} UAS-GFP/UAS-Gish*. (P) w; *esg-Gal4 tub-Gal80^{ts} UAS-GFP*; *UAS-Puc-RNAi*. (Q) w; *esg-Gal4 tub-Gal80^{ts} UAS-GFP/UAS-Gish*; *UAS-Puc-RNAi*.

Fig. 4

(A, E, and I) w; *esg-Gal4 tub-Gal80^{ts} UAS-GFP/+*. (B, F, and J) w; *esg-Gal4 tub-Gal80^{ts} UAS-GFP/+*; *UAS-gish-RNAi²⁸⁰⁶⁶*. (C, G, K) w; *esg-Gal4 tub-Gal80^{ts} UAS-GFP/UAS-Puc-RNAi*. (D, H, and L) w; *esg-Gal4 tub-Gal80^{ts} UAS-GFP/UAS-Puc-RNAi*; *UAS-gish-RNAi²⁸⁰⁶⁶*. (M) w; *esg-Gal4 tub-Gal80^{ts} UAS-GFP/UAS-Puc-RNAi*; *UAS-gish-RNAi²⁸⁰⁶⁶/UAS-Diap1*.

Fig. 5

(A) *esg-Gal4 tub-Gal80^{ts} UAS-GFP/+*. (B) w; *esg-Gal4 tub-Gal80^{ts} UAS-GFP/UAS-gish-RNAi¹⁰⁶⁸²⁶*. (C) w; *esg-Gal4 tub-Gal80^{ts} UAS-GFP/UAS-gish-RNAi¹⁰⁶⁸²⁶*; *UAS-Rho1-RNAi*. (E) w; *Myo1A-Gal4 tub-Gal80^{ts} UAS-GFP/+*. (F) w; *Myo1A-Gal4 tub-Gal80^{ts} UAS-GFP/UAS-gish-RNAi¹⁰⁶⁸²⁶*. (G) w; *Myo1A-Gal4 tub-Gal80^{ts} UAS-GFP/UAS-gish-RNAi¹⁰⁶⁸²⁶*; *UAS-Rho1-RNAi*. (I) w; *esg-Gal4*

tub-Gal80^{ts} UAS-GFP/+; puc-lacZ. (J) w; esg-Gal4 tub-Gal80^{ts} UAS-GFP/UAS-gish-RNAi¹⁰⁶⁸²⁶; puc-lacZ. (K) w; esg-Gal4 tub-Gal80^{ts} UAS-GFP/+; UAS-gish-RNAi¹⁰⁶⁸²⁶; UAS-Rho1-RNAi/puc-lacZ. (L) w; esg-Gal4 tub-Gal80^{ts} UAS-GFP/+; puc-lacZ. (M) w; esg-Gal4 tub-Gal80^{ts} UAS-GFP/+; UAS-Rho1^{V14}/puc-lacZ. (N) w; Myo1A-Gal4 tub-Gal80^{ts} UAS-GFP/+; puc-lacZ. (O) w; Myo1A-Gal4 tub-Gal80^{ts} UAS-GFP/+; UAS-Rho1^{V14}; puc-lacZ. (P) w; esg-Gal4 tub-Gal80^{ts} UAS-GFP/+. (Q) w; esg-Gal4 tub-Gal80^{ts} UAS-GFP/+; UAS-Rho1^{V14}.

Fig. 6

(A) esg-Gal4 tub-Gal80^{ts}/+ (esg^{ts}>yw), esg-Gal4 tub-Gal80^{ts}/UAS-gish-RNAi¹⁰⁶⁸²⁶ (esg^{ts}>Gish^{RNAi}), Myo1A-Gal4 tub-Gal80^{ts} UAS-GFP/+ (Myo^{ts}>yw), Myo1A-Gal4 tub-Gal80^{ts} UAS-GFP/UAS-gish-RNAi¹⁰⁶⁸²⁶ (Myo^{ts}>Gish^{RNAi}). (J) esg-Gal4 UAS-GFP/+; tub-Gal80^{ts}/+ (esg^{ts}>GFP), esg-Gal4 UAS-GFP/+; tub-Gal80^{ts}/UAS-Fg-Rho1 (esg^{ts}>GFP+Fg-Rho1), esg-Gal4 UAS-GFP/+; tub-Gal80^{ts}/UAS-Fg-Rho1^{SA} (esg^{ts}>GFP+Fg-Rho1^{SA}).

Fig. 7

(A–C') yw. (E–F') Rho1-GFP/+. (G and G') esg-Gal4 tub-Gal80^{ts}/UAS-Gish; Rho1-GFP/+. (H–I') yw; esg-Gal4 UAS-GFP tub-Gal80^{ts}/+; puc-lacZ/+. (J–J') yw; esg-Gal4 UAS-GFP tub-Gal80^{ts}/UAS-Fg-Gish; puc-lacZ/+. (H–L') yw; esg-Gal4 UAS-GFP tub-Gal80^{ts}/+. (M and M') yw; esg-Gal4 UAS-GFP tub-Gal80^{ts}/UAS-Fg-Gish.

Fig. S1

(A) w; esg-Gal4 tub-Gal80^{ts} UAS-GFP/+. (B) w; esg-Gal4 tub-Gal80^{ts} UAS-GFP/UAS-Gish-RNAi¹⁰⁶⁸²⁶. (C) w; esg-Gal4 tub-Gal80^{ts} UAS-GFP/+; UAS-Gish-RNAi²⁸⁰⁶⁶. (D) w; esg-Gal4 tub-Gal80^{ts} UAS-GFP/+; UAS-Gish-RNAi²⁶⁰⁰³. (F) w; esg-Gal4 tub-Gal80^{ts} UAS-GFP/+. (G) w; esg-Gal4 tub-Gal80^{ts} UAS-GFP/UAS-Gish-RNAi¹⁰⁶⁸²⁶. (H) w; esg-Gal4 tub-Gal80^{ts} UAS-GFP/UAS-Gish-RNAi¹⁰⁶⁸²⁶; UAS-Gish. (J) w; Myo1A-Gal4 tub-Gal80^{ts} UAS-GFP/+. (K) w; Myo1A-Gal4 tub-Gal80^{ts} UAS-GFP/UAS-Gish-RNAi¹⁰⁶⁸²⁶. (L) w; Myo1A-Gal4 tub-Gal80^{ts} UAS-GFP/UAS-Gish-RNAi¹⁰⁶⁸²⁶; UAS-Gish. (N) yw UAS-GFP hsf1p/+; tub-Gal4/+; FRT82B tub-Gal80/FRT82B. (O) yw UAS-GFP hsf1p/+; tub-Gal4/+; FRT82B tub-Gal80/FRT82B gish^{KG03891}. (P) yw UAS-GFP hsf1p/+; tub-Gal4/+; FRT82B tub-Gal80/FRT82B gish^{KG03891}; UAS-Myc-Gish^{WT}. (Q) yw UAS-GFP hsf1p/+; tub-Gal4/+; FRT82B tub-Gal80/FRT82B gish^{KG03891}; UAS-Gish^{KD}. (R) yw UAS-GFP hsf1p/+; tub-Gal4/+; FRT82B tub-Gal80/FRT82B gish^{KG03891}; UAS-Gish^{ΔC}.

Fig. S2

(A) w; esg-Gal4 tub-Gal80^{ts} UAS-GFP/+. (B) w; esg-Gal4 tub-Gal80^{ts} UAS-GFP/UAS-Gish-RNAi¹⁰⁶⁸²⁶. (C) w; esg-Gal4 tub-Gal80^{ts} UAS-GFP/UAS-Gish-RNAi¹⁰⁶⁸²⁶; UAS-Yki-RNAi.

Fig. S3

(A–A'') w; esg-Gal4 tub-Gal80^{ts} UAS-GFP/+; puc-lacZ. (B) w; esg-Gal4 tub-Gal80^{ts} UAS-GFP/UAS-Gish-RNAi¹⁰⁶⁸²⁶; puc-lacZ. (D and H) MS1096. (E, E', and I) puc^{E69}/+. (C and J) MS1096; UAS-Gish-RNAi¹⁰⁶⁸²⁶. (G, G', and K) MS1096; UAS-Gish-RNAi¹⁰⁶⁸²⁶; puc^{E69}/+.

Fig. S4

(A) w; MyoGal4 tub-Gal80^{ts} UAS-GFP. (B) w; MyoGal4 tub-Gal80^{ts} UAS-GFP; UAS-Gish-RNAi. (C) UAS-BSK^{DN}; MyoGal4 tub-Gal80^{ts} UAS-GFP. (D) UAS-BSK^{DN}; MyoGal4 tub-Gal80^{ts} UAS-GFP; UAS-Gish-RNAi. (H) w; esg-Gal4 tub-Gal80^{ts} UAS-GFP. (I) w; esg-Gal4 tub-Gal80^{ts} UAS-GFP/UAS-Gish-RNAi. (J) w; esg-Gal4 tub-Gal80^{ts} UAS-GFP; UAS-DIAP1. (K) w; esg-Gal4 tub-Gal80^{ts} UAS-GFP/UAS-Gish-RNAi; UAS-DIAP1. (M) w; MyoGal4 tub-Gal80^{ts} UAS-GFP. (N) w; MyoGal4 tub-Gal80^{ts} UAS-GFP/UAS-Gish-RNAi. (O) w; MyoGal4 tub-Gal80^{ts} UAS-GFP; UAS-DIAP1. (P) w; MyoGal4 tub-Gal80^{ts} UAS-GFP/UAS-Gish-RNAi; UAS-DIAP1.

Fig. S5

(A–A'') hh-Gal4/Rho1-GFP. (B–B'') UAS-Gish-RNAi¹⁰⁶⁸²⁶; Hh-Gal4/Rho1-GFP.

Online supplemental material

Fig. S1 shows that Gish restricts ISC proliferation through its kinase activity and membrane association. Fig. S2 shows that knockdown of Yki did not rescue ISC overproliferation caused by Gish RNAi. Fig. S3 shows that Gish knockdown activated JNK pathway in midgut progenitor cells as well as in wing imaginal discs and that Gish knockdown synergized with puc heterozygosity to induce apoptosis in developing wings. Fig. S4 shows that Gish knockdown promoted ISC proliferation through both JNK pathway and apoptosis. Fig. S5 shows that Gish knockdown increased Rho-GFP level in wing imaginal discs.

Acknowledgments

We are grateful to Dr. Ronald Davis (Scripps Research, Jupiter, FL) for kindly providing Gish antibody, Bloomington and VDRC stock centers for fly strains, and Developmental Studies Hybridoma Bank for antibodies.

This work was supported by grants from the National Institutes of Health (GM118063) and Welch Foundation (I-1603) to J. Jiang. J. Jiang is a Eugene McDermott Endowed Scholar in Biomedical Science at the University of Texas Southwestern.

The authors declare no competing financial interests.

Author contributions: Conceptualization, J. Jiang. Methodology, Shuangxi Li, A. Tian, Shuang Li, Y. Han, and B. Wang. Investigation, Shuangxi Li, A. Tian, Shuang Li, Y. Han, and B. Wang. Resources, J. Jiang. Writing, J. Jiang. Visualization, Shuangxi Li, A. Tian, Shuang Li, and Y. Han. Funding acquisition, J. Jiang. Supervision, J. Jiang.

Submitted: 17 September 2019

Revised: 3 January 2020

Accepted: 16 January 2020

References

- Amcheslavsky, A., J. Jiang, and Y.T. Ip. 2009. Tissue damage-induced intestinal stem cell division in *Drosophila*. *Cell Stem Cell* 4:49–61. <https://doi.org/10.1016/j.stem.2008.10.016>
- Bach, E.A., L.A. Ekas, A. Ayala-Camargo, M.S. Flaherty, H. Lee, N. Perrimon, and G.H. Baeg. 2007. GFP reporters detect the activation of the

- Drosophila JAK/STAT pathway in vivo. *Gene Expr. Patterns*. 7:323–331. <https://doi.org/10.1016/j.modgep.2006.08.003>
- Beehler-Evans, R., and C.A. Micchelli. 2015. Generation of enteroendocrine cell diversity in midgut stem cell lineages. *Development*. 142:654–664. <https://doi.org/10.1242/dev.114959>
- Bischof, J., R.K. Maeda, M. Hediger, F. Karch, and K. Basler. 2007. An optimized transgenesis system for Drosophila using germ-line-specific phiC31 integrases. *Proc. Natl. Acad. Sci. USA*. 104:3312–3317. <https://doi.org/10.1073/pnas.0611511104>
- Biteau, B., C.E. Hochmuth, and H. Jasper. 2008. JNK activity in somatic stem cells causes loss of tissue homeostasis in the aging Drosophila gut. *Cell Stem Cell*. 3:442–455. <https://doi.org/10.1016/j.stem.2008.07.024>
- Biteau, B., C.E. Hochmuth, and H. Jasper. 2011. Maintaining tissue homeostasis: dynamic control of somatic stem cell activity. *Cell Stem Cell*. 9: 402–411. <https://doi.org/10.1016/j.stem.2011.10.004>
- Biteau, B., and H. Jasper. 2011. EGF signaling regulates the proliferation of intestinal stem cells in Drosophila. *Development*. 138:1045–1055. <https://doi.org/10.1242/dev.056671>
- Biteau, B., and H. Jasper. 2014. Slit/Robo signaling regulates cell fate decisions in the intestinal stem cell lineage of Drosophila. *Cell Rep*. 7:1867–1875. <https://doi.org/10.1016/j.celrep.2014.05.024>
- Buchon, N., N.A. Broderick, S. Chakrabarti, and B. Lemaitre. 2009. Invasive and indigenous microbiota impact intestinal stem cell activity through multiple pathways in Drosophila. *Genes Dev*. 23:2333–2344. <https://doi.org/10.1101/gad.1827009>
- Buchon, N., D. Osman, F.P. David, H.Y. Fang, J.P. Boquete, B. Deplancke, and B. Lemaitre. 2013. Morphological and molecular characterization of adult midgut compartmentalization in Drosophila. *Cell Rep*. 3:1725–1738. <https://doi.org/10.1016/j.celrep.2013.04.001>
- Chen, J., N. Xu, C. Wang, P. Huang, H. Huang, Z. Jin, Z. Yu, T. Cai, R. Jiao, and R. Xi. 2018. Transient Scute activation via a self-stimulatory loop directs enteroendocrine cell pair specification from self-renewing intestinal stem cells. *Nat. Cell Biol*. 20:152–161. <https://doi.org/10.1038/s41556-017-0020-0>
- Cho, Y.S., J. Zhu, S. Li, B. Wang, Y. Han, and J. Jiang. 2018. Regulation of Yki/Yap subcellular localization and Hpo signaling by a nuclear kinase PRP4K. *Nat. Commun*. 9:1657. <https://doi.org/10.1038/s41467-018-04090-2>
- Cordero, J.B., R.K. Stefanatos, A. Scopelliti, M. Vidal, and O.J. Sansom. 2012. Inducible progenitor-derived Wingless regulates adult midgut regeneration in Drosophila. *EMBO J*. 31:3901–3917. <https://doi.org/10.1038/emboj.2012.248>
- Gault, W.J., P. Olguin, U. Weber, and M. Mlodzik. 2012. Drosophila CK1-γ, gilgamesh, controls PCP-mediated morphogenesis through regulation of vesicle trafficking. *J. Cell Biol*. 196:605–621. <https://doi.org/10.1083/jcb.201107137>
- Goulas, S., R. Conder, and J.A. Knoblich. 2012. The Par complex and integrins direct asymmetric cell division in adult intestinal stem cells. *Cell Stem Cell*. 11:529–540. <https://doi.org/10.1016/j.stem.2012.06.017>
- Gregory, S.L., T. Shandala, L. O'Keefe, L. Jones, M.J. Murray, and R. Saint. 2007. A Drosophila overexpression screen for modifiers of Rho signalling in cytokinesis. *Fly (Austin)*. 1:13–22. <https://doi.org/10.4161/fly.3806>
- Guo, Z., I. Driver, and B. Ohlstein. 2013. Injury-induced BMP signaling negatively regulates Drosophila midgut homeostasis. *J. Cell Biol*. 201: 945–961. <https://doi.org/10.1083/jcb.201302049>
- Hodge, R.G., and A.J. Ridley. 2016. Regulating Rho GTPases and their regulators. *Nat. Rev. Mol. Cell Biol*. 17:496–510. <https://doi.org/10.1038/nrm.2016.67>
- Jiang, H., and B.A. Edgar. 2012. Intestinal stem cell function in Drosophila and mice. *Curr. Opin. Genet. Dev*. 22:354–360. <https://doi.org/10.1016/j.gde.2012.04.002>
- Jiang, H., M.O. Grenley, M.J. Bravo, R.Z. Blumhagen, and B.A. Edgar. 2011. EGFR/Ras/MAPK signaling mediates adult midgut epithelial homeostasis and regeneration in Drosophila. *Cell Stem Cell*. 8:84–95. <https://doi.org/10.1016/j.stem.2010.11.026>
- Jiang, H., P.H. Patel, A. Kohlmaier, M.O. Grenley, D.G. McEwen, and B.A. Edgar. 2009. Cytokine/Jak/Stat signaling mediates regeneration and homeostasis in the Drosophila midgut. *Cell*. 137:1343–1355. <https://doi.org/10.1016/j.cell.2009.05.014>
- Jiang, H., A. Tian, and J. Jiang. 2016. Intestinal stem cell response to injury: lessons from Drosophila. *Cell. Mol. Life Sci*. 73:3337–3349. <https://doi.org/10.1007/s00018-016-2235-9>
- Karpowicz, P., J. Perez, and N. Perrimon. 2010. The Hippo tumor suppressor pathway regulates intestinal stem cell regeneration. *Development*. 137: 4135–4145. <https://doi.org/10.1242/dev.060483>
- Knippschild, U., A. Gocht, S. Wolff, N. Huber, J. Löhler, and M. Stöter. 2005. The casein kinase 1 family: participation in multiple cellular processes in eukaryotes. *Cell. Signal*. 17:675–689. <https://doi.org/10.1016/j.cellsig.2004.12.011>
- Lee, T., and L. Luo. 2001. Mosaic analysis with a repressible cell marker (MARCM) for Drosophila neural development. *Trends Neurosci*. 24: 251–254. [https://doi.org/10.1016/S0166-2236\(00\)01791-4](https://doi.org/10.1016/S0166-2236(00)01791-4)
- Lee, W.C., K. Beebe, L. Sudmeier, and C.A. Micchelli. 2009. Adenomatous polyposis coli regulates Drosophila intestinal stem cell proliferation. *Development*. 136:2255–2264. <https://doi.org/10.1242/dev.035196>
- Li, Q., S. Li, S. Mana-Capelli, R.J. Roth Flach, L.V. Danai, A. Amcheslavsky, Y. Nie, S. Kaneko, X. Yao, X. Chen, et al. 2014a. The conserved misshapen-warts-Yorkie pathway acts in enteroblasts to regulate intestinal stem cells in Drosophila. *Dev. Cell*. 31:291–304. <https://doi.org/10.1016/j.devcel.2014.09.012>
- Li, S., Y.S. Cho, T. Yue, Y.T. Ip, and J. Jiang. 2015. Overlapping functions of the MAP4K family kinases Hppy and Msn in Hippo signaling. *Cell Discov*. 1: 15038. <https://doi.org/10.1038/celldisc.2015.38>
- Li, S., S. Li, Y. Han, C. Tong, B. Wang, Y. Chen, and J. Jiang. 2016. Regulation of Smoothened phosphorylation and high-level Hedgehog signaling activity by a plasma membrane associated kinase. *PLoS Biol*. 14:e1002481. <https://doi.org/10.1371/journal.pbio.1002481>
- Li, Z., Y. Guo, L. Han, Y. Zhang, L. Shi, X. Huang, and X. Lin. 2014b. Debra-mediated Ci degradation controls tissue homeostasis in Drosophila adult midgut. *Stem Cell Rep*. 2:135–144. <https://doi.org/10.1016/j.stemcr.2013.12.011>
- Li, Z., Y. Zhang, L. Han, L. Shi, and X. Lin. 2013. Trachea-derived dpp controls adult midgut homeostasis in Drosophila. *Dev. Cell*. 24:133–143. <https://doi.org/10.1016/j.devcel.2012.12.010>
- Liu, J., and A. Lin. 2005. Role of JNK activation in apoptosis: a double-edged sword. *Cell Res*. 15:36–42. <https://doi.org/10.1038/sj.cr.7290262>
- Marianes, A., and A.C. Spradling. 2013. Physiological and stem cell compartmentalization within the Drosophila midgut. *eLife*. 2:e00886. <https://doi.org/10.7554/eLife.00886>
- Martín-Blanco, E., A. Gampel, J. Ring, K. Virdee, N. Kirov, A.M. Tolkovsky, and A. Martínez-Arias. 1998. puckered encodes a phosphatase that mediates a feedback loop regulating JNK activity during dorsal closure in Drosophila. *Genes Dev*. 12:557–570. <https://doi.org/10.1101/gad.12.4.557>
- McGuire, S.E., Z. Mao, and R.L. Davis. 2004. Spatiotemporal gene expression targeting with the TARGET and gene-switch systems in Drosophila. *Sci. STKE*. 2004:pl6.
- Micchelli, C.A., and N. Perrimon. 2006. Evidence that stem cells reside in the adult Drosophila midgut epithelium. *Nature*. 439:475–479. <https://doi.org/10.1038/nature04371>
- Moreno, E., M. Yan, and K. Basler. 2002. Evolution of TNF signaling mechanisms: JNK-dependent apoptosis triggered by Eiger, the Drosophila homolog of the TNF superfamily. *Curr. Biol*. 12:1263–1268. [https://doi.org/10.1016/S0960-9822\(02\)00954-5](https://doi.org/10.1016/S0960-9822(02)00954-5)
- Neisch, A.L., O. Speck, B. Stronach, and R.G. Fehon. 2010. Rho1 regulates apoptosis via activation of the JNK signaling pathway at the plasma membrane. *J. Cell Biol*. 189:311–323. <https://doi.org/10.1083/jcb.200912010>
- Ohlstein, B., and A. Spradling. 2006. The adult Drosophila posterior midgut is maintained by pluripotent stem cells. *Nature*. 439:470–474. <https://doi.org/10.1038/nature04333>
- Ohlstein, B., and A. Spradling. 2007. Multipotent Drosophila intestinal stem cells specify daughter cell fates by differential notch signaling. *Science*. 315:988–992. <https://doi.org/10.1126/science.1136606>
- Patel, P.H., D. Dutta, and B.A. Edgar. 2015. Niche appropriation by Drosophila intestinal stem cell tumours. *Nat. Cell Biol*. 17:1182–1192. <https://doi.org/10.1038/ncb3214>
- Ren, F., Q. Shi, Y. Chen, A. Jiang, Y.T. Ip, H. Jiang, and J. Jiang. 2013. Drosophila Myc integrates multiple signaling pathways to regulate intestinal stem cell proliferation during midgut regeneration. *Cell Res*. 23: 1133–1146. <https://doi.org/10.1038/cr.2013.101>
- Ren, F., B. Wang, T. Yue, E.Y. Yun, Y.T. Ip, and J. Jiang. 2010. Hippo signaling regulates Drosophila intestine stem cell proliferation through multiple pathways. *Proc. Natl. Acad. Sci. USA*. 107:21064–21069. <https://doi.org/10.1073/pnas.1012759107>
- Sarov, M., C. Barz, H. Jambor, M.Y. Hein, C. Schmied, D. Suchold, B. Stender, S. Janosch, V.V. Konakondla-Jacob, R.T. Krishnan, et al. 2016. A genome-wide resource for the analysis of protein localisation in Drosophila. *eLife*. 5:e12068. <https://doi.org/10.7554/eLife.12068>
- Shaw, R.L., A. Kohlmaier, C. Polesello, C. Veelken, B.A. Edgar, and N. Tapon. 2010. The Hippo pathway regulates intestinal stem cell proliferation

- during *Drosophila* adult midgut regeneration. *Development*. 137: 4147–4158. <https://doi.org/10.1242/dev.052506>
- Staley, B.K., and K.D. Irvine. 2010. Warts and Yorkie mediate intestinal regeneration by influencing stem cell proliferation. *Curr. Biol.* 20: 1580–1587. <https://doi.org/10.1016/j.cub.2010.07.041>
- Tan, Y., D. Yu, J. Pletting, and R.L. Davis. 2010. Gilgamesh is required for rutabaga-independent olfactory learning in *Drosophila*. *Neuron*. 67: 810–820. <https://doi.org/10.1016/j.neuron.2010.08.020>
- Tian, A., and J. Jiang. 2014. Intestinal epithelium-derived BMP controls stem cell self-renewal in *Drosophila* adult midgut. *eLife*. 3:e01857. <https://doi.org/10.7554/eLife.01857>
- Tian, A., and J. Jiang. 2017. Dual role of BMP signaling in the regulation of *Drosophila* intestinal stem cell self-renewal. *Fly (Austin)*. 11:297–302. <https://doi.org/10.1080/19336934.2017.1384104>
- Tian, A., Q. Shi, A. Jiang, S. Li, B. Wang, and J. Jiang. 2015. Injury-stimulated Hedgehog signaling promotes regenerative proliferation of *Drosophila* intestinal stem cells. *J. Cell Biol.* 208:807–819. <https://doi.org/10.1083/jcb.201409025>
- Tian, A., B. Wang, and J. Jiang. 2017. Injury-stimulated and self-restrained BMP signaling dynamically regulates stem cell pool size during *Drosophila* midgut regeneration. *Proc. Natl. Acad. Sci. USA*. 114:E2699–E2708. <https://doi.org/10.1073/pnas.1617790114>
- Tillement, V., I. Lajoie-Mazenc, A. Casanova, C. Froment, M. Penary, D. To-var, R. Marquez, B. Monsarrat, G. Favre, and A. Pradines. 2008. Phosphorylation of RhoB by CK1 impedes actin stress fiber organization and epidermal growth factor receptor stabilization. *Exp. Cell Res.* 314: 2811–2821. <https://doi.org/10.1016/j.yexcr.2008.06.011>
- Tong, C., and J. Jiang. 2007. Using immunoprecipitation to study protein-protein interactions in the Hedgehog-signaling pathway. *Methods Mol. Biol.* 397:215–229. https://doi.org/10.1007/978-1-59745-516-9_15
- Wang, G., B. Wang, and J. Jiang. 1999. Protein kinase A antagonizes Hedgehog signaling by regulating both the activator and repressor forms of *Cubitus interruptus*. *Genes Dev.* 13:2828–2837. <https://doi.org/10.1101/gad.13.21.2828>
- Weber, U., N. Paricio, and M. Mlodzik. 2000. Jun mediates Frizzled-induced R3/R4 cell fate distinction and planar polarity determination in the *Drosophila* eye. *Development*. 127:3619–3629.
- Wei, J., R.K. Mialki, S. Dong, A. Khoo, R.K. Mallampalli, Y. Zhao, and J. Zhao. 2013. A new mechanism of RhoA ubiquitination and degradation: roles of SCF(FBXL19) E3 ligase and Erk2. *Biochim. Biophys. Acta*. 1833: 2757–2764. <https://doi.org/10.1016/j.bbamcr.2013.07.005>
- Xu, N., S.Q. Wang, D. Tan, Y. Gao, G. Lin, and R. Xi. 2011. EGFR, Wingless and JAK/STAT signaling cooperatively maintain *Drosophila* intestinal stem cells. *Dev. Biol.* 354:31–43. <https://doi.org/10.1016/j.ydbio.2011.03.018>
- Zeng, X., C. Chauhan, and S.X. Hou. 2010. Characterization of midgut stem cell- and enteroblast-specific Gal4 lines in *Drosophila*. *Genesis*. 48: 607–611. <https://doi.org/10.1002/dvg.20661>
- Zeng, X., and S.X. Hou. 2015. Enteroendocrine cells are generated from stem cells through a distinct progenitor in the adult *Drosophila* posterior midgut. *Development*. 142:644–653. <https://doi.org/10.1242/dev.113357>
- Zhang, L., F. Ren, Q. Zhang, Y. Chen, B. Wang, and J. Jiang. 2008. The TEAD/TEF family of transcription factor Scalloped mediates Hippo signaling in organ size control. *Dev. Cell*. 14:377–387. <https://doi.org/10.1016/j.devcel.2008.01.006>

Supplemental material

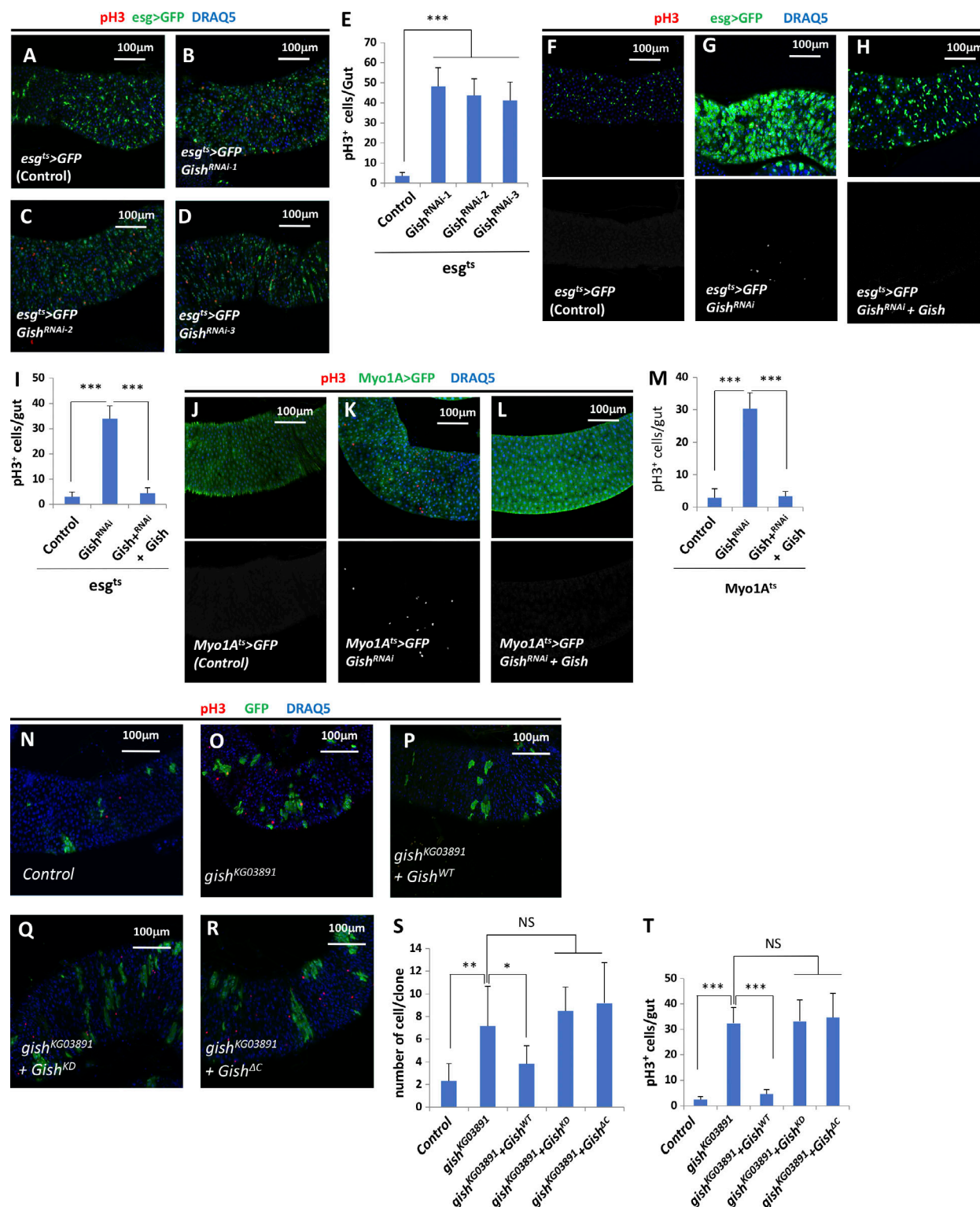


Figure S1. **Gish restricts ISC proliferation through its kinase activity and membrane association.** (A–E) Adult midguts expressing the indicated *Gish* RNAi lines in progenitor cells (A–D) were immunostained for pH3 and GFP. Quantification of pH3⁺ cells is shown in E. *n* = 30 guts for each genotype. Data are mean ± SD. ****P* < 0.001 (Student's *t* test). (F–M) pH3 staining in adult midguts of the indicated genotypes. Quantification of pH3⁺ cells is shown in I and M. *n* = 20 guts for each genotype. Data are mean ± SD. ****P* < 0.001 (Student's *t* test). (N–R) Midguts containing MACRM clones for *FRT82B* control (N) or *FRT82B gish^{KG03891}* without (O) or with transgenic expression of a WT *Gish* (P), a kinase-dead *Gish* (Q), or a C-terminally truncated *Gish* (R) were immunostained for pH3 (red) GFP (green), and DRAQ5 (blue). (S and T) Quantification of clone size (S) and number of pH3⁺ cells (T) in guts containing the indicated MACRM clones. *n* = 15 guts for each genotype. Data are mean ± SD. **P* < 0.05, ***P* < 0.01, ****P* < 0.001 (Student's *t* test).

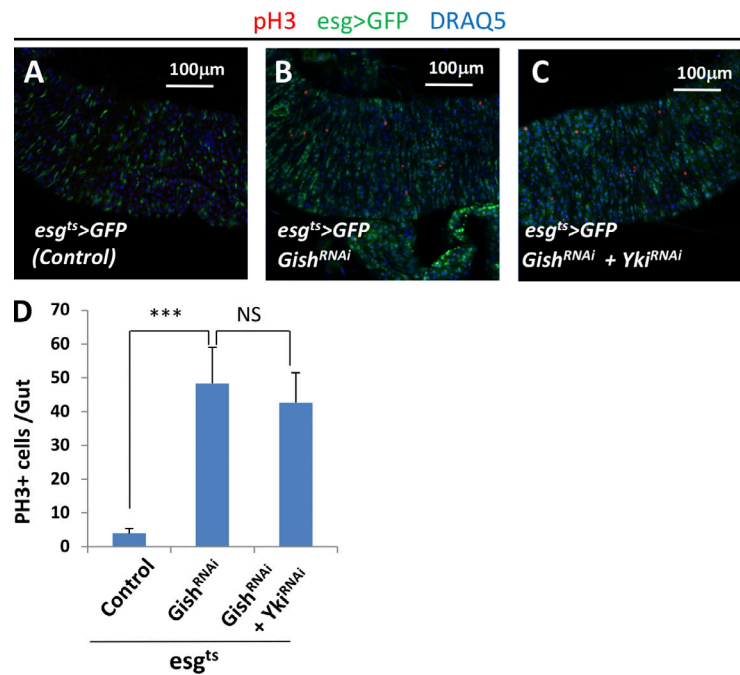


Figure S2. **Knockdown of Yki did not rescue ISC overproliferation caused by Gish RNAi.** (A–C) Expression of pH3 (red), GFP (green), and DRAQ5 (blue) in control guts (A), Gish RNA guts (B), or Gish Yki double RNAi guts (C). (D) Quantification of pH3⁺ cells in adult midguts of the indicated genotypes. *n* = 20 guts for each genotype. Data are mean ± SD. ****P* < 0.001 (Student's *t* test).

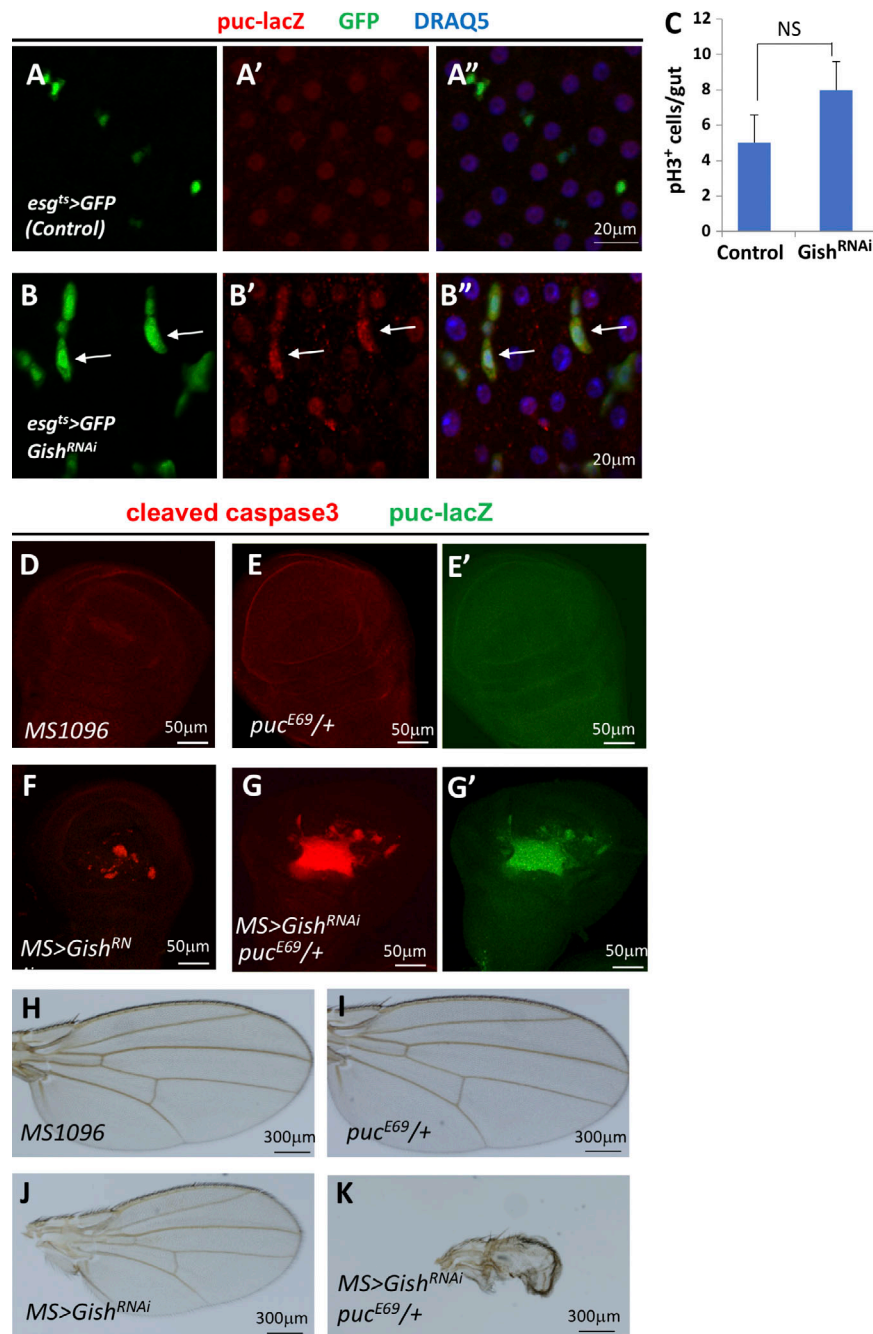


Figure S3. **Gish knockdown activated JNK pathway.** (A–B') 2–3-d-old adult females of *esg^{ts}* control or *esg^{ts}>Gish^{RNAi}* were shifted to 29°C for 3 d, followed by immunostaining for GFP, pH3, and DRAQ5. (C) Quantification of pH3⁺ cells in control guts or guts expressing *esg^{ts}>Gish^{RNAi}* for 3 d. *n* = 15 guts for each genotype. Data are mean ± SD. (D–G') Wing imaginal discs of the indicated genotypes were immunostaining for activated caspase-3 (red) and *puc-lacZ* (green). *UAS-Gish-RNAi* was driven by the wing-specific Gal4 driver *MS1096*. (H–K) Adult wings of the indicated genotypes. *UAS-Gish-RNAi* was driven by the wing-specific Gal4 driver *MS1096*.

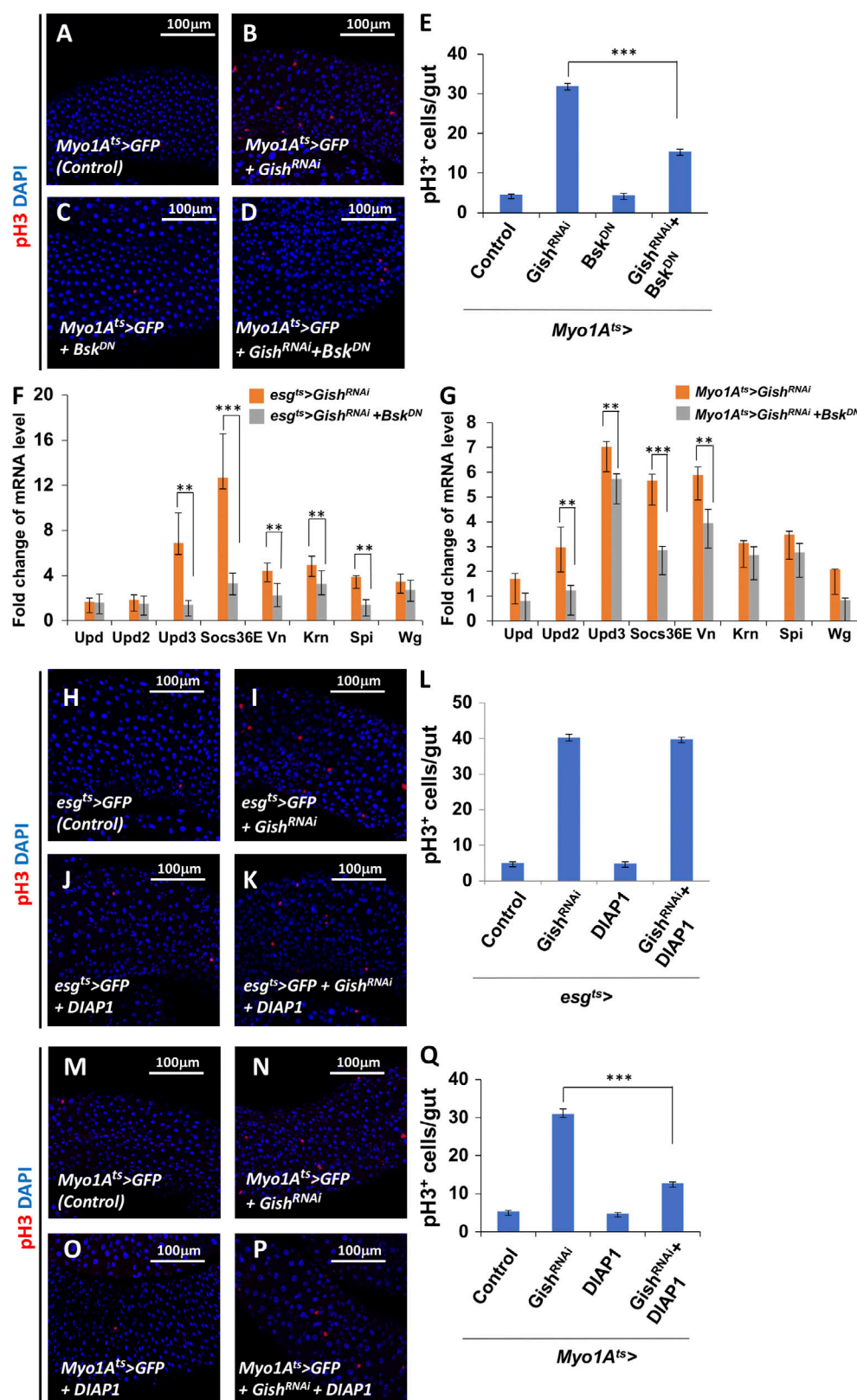


Figure S4. **Gish knockdown promoted ISC proliferation through JNK pathway and apoptosis.** (A-E) Adult midguts of the indicated genotypes (A-D) were immunostained for pH3 and DAPI. Quantification of pH3⁺ cells is shown in E. *n* = 10 guts for each genotype. Data are mean ± SD from three independent experiments. ****P* < 0.001 (Student's *t* test). (F and G) mRNA levels of JAK-STAT, EGFR, and Wg pathway components in adult midguts of the indicated genotypes. Numbers on y axis indicate fold change normalized by control guts. Data are mean ± SD. ***P* < 0.01, ****P* < 0.001 (Student's *t* test). (H-K and M-P) Adult midguts of the indicated genotypes were immunostained for pH3 and DAPI. (L and Q) Quantification of pH3⁺ cells in adult midguts of the indicated genotypes. *n* = 10 guts for each genotype. Data are mean ± SD from three independent experiments. ****P* < 0.001 (Student's *t* test).

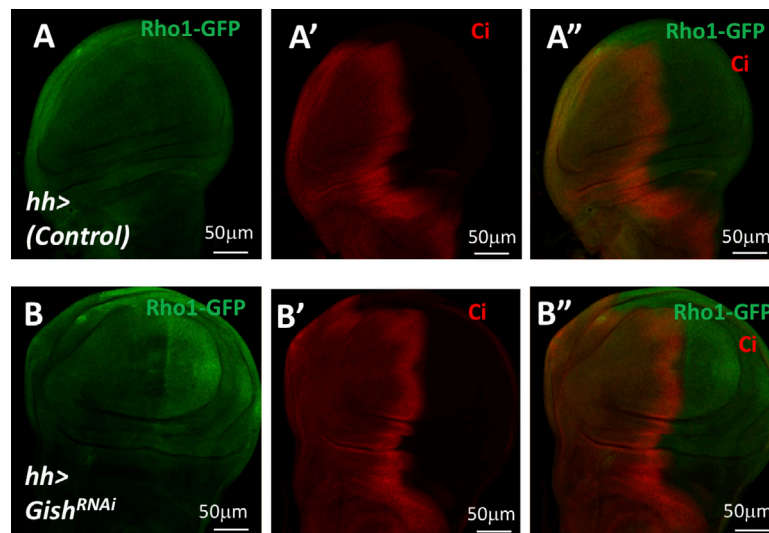


Figure S5. **Gish knockdown increased Rho-GFP level.** (A–B'') Control wing discs (*hh-Gal4*; A–A'') or wing discs expressing *UAS-Gish-RNAi* under the control of *hh-Gal4* (B–B'') were immunostained for Ci (red) and Rho-GFP (green). *hh-Gal4* drives *UAS* transgene expression in P-compartment cells marked by the lack of Ci expression.